AD-A114 637 SCRIPPS INSTITUTION OF OCEANOGRAPHY LA JOLLA CA VISA--ETC F/G 4/1
AIRBORNE MEASUREMENTS OF EUROPEAN SKY AND TERRAIN RADIANCES.(U)
AUG 81 R W JOHNSON F19628-78-C-0200
UNCLASSIFIED SIO-82-2 AFGL-TR-81-0275 NL

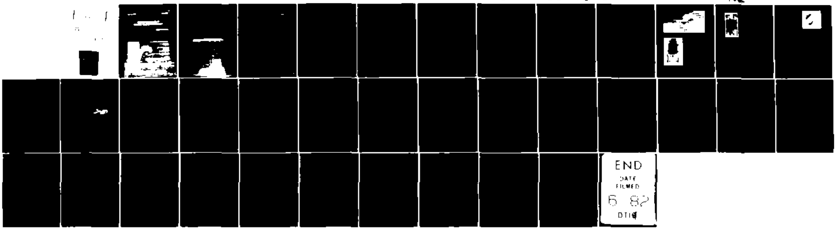

END
DATE
FILMED
6 82
DTIC

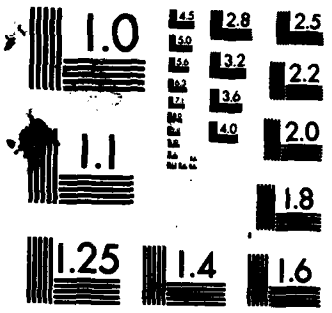
1.0
1.1
1.25
1.4
1.6
1.8
2.0
2.2
2.5
2.8
3.2
3.6
4.0
4.5
5.0
5.6
6.3

UNCLASSIFIED
SECURITY CLASSIFICATION OF THIS PAGE (When Data Entered)

REPORT DOCUMENTATION PAGE

READ INSTRUCTIONS BEFORE COMPLETING FORM

1. REPORT NUMBER AFGL-TR-81-0275	2. GOVT ACCESSION NO. AD-A114 637
3. RECIPIENT'S CATALOG NUMBER	
4. TITLE (and Subtitle) AIRBORNE MEASUREMENTS OF EUROPEAN SKY AND TERRAIN RADIANCES	5. TYPE OF REPORT & PERIOD COVERED Scientific - Interim Scientific Report No. 19
	6. PERFORMING ORG. REPORT NUMBER SIO Ref. 82-2
7. AUTHOR(s) Richard W. Johnson	8. CONTRACT OR GRANT NUMBER(s) F19628-78-C-0200
9. PERFORMING ORGANIZATION NAME AND ADDRESS University of California, San Diego Visibility Laboratory La Jolla, California 92093	10. PROGRAM ELEMENT, PROJECT, TASK AREA & WORK UNIT NUMBERS 62101F 7670-14-01
11. CONTROLLING OFFICE NAME AND ADDRESS Air Force Geophysics Laboratory Hanscom AFB, Massachusetts 01731 Contract Monitor: Major John D. Mill/OPA	12. REPORT DATE August 1981
	13. NUMBER OF PAGES 35
14. MONITORING AGENCY NAME & ADDRESS (if different from Controlling Office)	15. SECURITY CLASS. (of this report) UNCLASSIFIED
	15a. DECLASSIFICATION/DOWNGRADING SCHEDULE

16. DISTRIBUTION STATEMENT (of this Report)

Approved for public release; distribution unlimited.

17. DISTRIBUTION STATEMENT (of the abstract entered in Block 20, if different from Report)

18. SUPPLEMENTARY NOTES

19. KEY WORDS (Continue on reverse side if necessary and identify by block number)

Clear Sky Radiances
Terrain Radiance
Atmospheric Optical Properties
Cloudy Sky Radiances

20. ABSTRACT (Continue on reverse side if necessary and identify by block number)

A data set which contains nearly 500 arrays representing measurements of sky and terrain radiance values from 47 different flights is described and illustrated. The measurements were made using radiometer systems mounted on a C-130 aircraft during a series of European flights associated with the NATO program OPAQUE, Fenn (1978) and Johnson *et al.* (1979).

Radiance measurements throughout the $\overset{pi}{4\pi}$ field surrounding the aircraft were made in — over

20. ABSTRACT continued:

four spectral bands having mean wavelengths of 478, 557, 664 and 765nm. Spectral sets of measurements were made at each of several altitudes between the surface and approximately 6 km AGL.

Evaluation of the data illustrates good orientation and radiometric accuracies, except for stray light influences as the radiometer field of view swept near and through the solar disc. Corrective procedures are outlined and their application is undergoing further refinement.

These data are appropriate for use in the development of operationally useful predictive models. ~~as illustrated in Hering (1981).~~ The radiance data in conjunction with their companion scattering coefficient data ~~(Johnson and Gordon (1980))~~ are readily applicable to the determination of slant path contrast transmittances, atmospheric optical depths, aerosol directional scattering characteristics, flux divergences and their attendant determinations of turbid atmospheric single scattering albedos.

AFGL-TR-81-0275 **SIO Ref. 82-2**

AIRBORNE MEASUREMENTS OF EUROPEAN SKY AND TERRAIN RADIANCES

Richard W. Johnson

Visibility Laboratory
University of California, San Diego
Scripps Institution of Oceanography
La Jolla, California 92093

Approved:

Roswell W. Austin, Director
Visibility Laboratory

Approved:

William A. Nierenberg, Director
Scripps Institution of Oceanography

CONTRACT NO. F19628-78-C-0200
Project No. 7670
Task No. 7670-14
Work Unit No. 7670-14-01

Scientific Report No. 19
August 1981

Contract Monitor
Major John D. Mill, Atmospheric Optics Branch, Optical Physics Division

Approved for public release; distribution unlimited.

Prepared for

AIR FORCE GEOPHYSICS LABORATORY
AIR FORCE SYSTEMS COMMAND
UNITED STATES AIR FORCE
HANSCOM AFB, MASSACHUSETTS 01731

SUMMARY

A data set which contains nearly 500 arrays representing measurements of sky and terrain radiance values is described and illustrated. The measurements were made using radiometer systems mounted on a C-130 aircraft during a series of European flights associated with the NATO program OPAQUE, Fenn (1978) and Johnson *et al.* (1979).

Radiance measurements throughout the 4π field surrounding the aircraft were made in four spectral bands having mean wavelengths of 478, 557, 664 and 765nm. Spectral sets of measurements were made at each of several altitudes between the surface and approximately 6 km AGL.

Evaluation of the data illustrates good orientation and radiometric accuracies, except for stray light influences as the radiometer field of view swept near and through the solar disc. Corrective procedures are outlined and their application is undergoing further refinement.

These data are appropriate for use in the development of operationally useful predictive models as illustrated in Hering (1981). The radiance data in conjunction with their companion scattering coefficient data, Johnson and Gordon (1980) are readily applicable to the determination of slant path contrast transmittances, atmospheric optical depths, aerosol directional scattering characteristics, flux divergences and their attendant determinations of turbid atmospheric single scattering albedos.

TABLE OF CONTENTS

LIST OF TABLES AND ILLUSTRATIONS

AIRBORNE MEASUREMENTS OF EUROPEAN SKY AND TERRAIN RADIANCES

Richard W. Johnson

1. INTRODUCTION

As the ever broadening world of electro-optical search and detection continues to impose its technical influence upon our most imaginative operational scenarios, it behooves us to be assured of our abilities to fully understand, and hopefully to accurately model the characterization of these operational environments. It is in support of this general context that the Visibility Laboratory in cooperation with, and under the sponsorship of the Air Force Geophysics Laboratory has maintained an extensive program of airborne optical and meteorological measurements. Many of these data, all of which were directed toward enhancing our understanding the fundamental elements of contrast transmittance through the troposphere, have been presented in several earlier technical reports, among them being Duntley, *et al.* (1976), Johnson, *et al.* (1979), Johnson and Gordon (1980) and Johnson (1981).

Whereas the most recent of the reports referenced above have concentrated upon the documentation and modelling of the vertical structure of the atmospheric volume scattering coefficient, it is important to note that there is a substantial and valuable complementary data set associated with each of these flight episodes that has not been made readily available to the user community. This complementary data set includes angularly precise spectral measurements of the 4π radiance field surrounding the aircraft at several different altitudes throughout the zero to six kilometer altitude regime. The possession of these radiance data is what enables one to characterize a broad variety of the environmental conditions extant during the flight episode and thus lead to the development of operationally useful predictive models. The radiance data in conjunction with their companion scattering coefficient data are readily applicable to the determination of slant path contrast transmittances, atmospheric optical depths, aerosol directional scattering characteristics, flux divergences and their attendant determinations of turbid atmosphere single scattering albedos.

The presentation of selected sets of these 4π radiance distributions, and a discussion of several pertinent characteristics of the data and its application are the subjects of this report.

2. DATA COLLECTION SYSTEM

The airborne data collection system that was used to collect the measurements presented and discussed in this report has been described previously. Each of the data reports listed in Appendix C discusses the general characteristics of the specific optical-meteorological sub-systems appropriate to that report's data. Similarly, the following paragraphs will briefly review the pertinent characteristics of the Automatic 2π Scanner Assemblies, the primary instruments related to the data presented in this report.

An annotated illustration of the total airborne instrument system as it appeared during a 1977 deployment to Lorient, France is shown in Fig. 2-1. Attention should be drawn to the Upper and Lower Hemisphere Scanner locations and the corresponding locations of their companion camera systems. A more detailed view of an Automatic Scanner Assembly, two of which are mounted on the aircraft, is shown in Fig. 2-2. In this view the instrument has been removed from the aircraft and is attached to its ground storage rack.

The scanner assembly illustrated in Fig. 2-2 is essentially a servo-following telescope assembly associated with both an optical filter selector and a photomultiplier detector. The mechanical orientations associated with these basic sub-assemblies are illustrated in Fig. 2-3 which is an annotated outline drawing of the composite assembly.

The azimuth and elevation drives in the 2π Scanner system are servo follower devices whose power and control circuits reside inside the cargo compartment of the aircraft where their performance can be monitored by the flight crew. A typical installation of the control console is shown in Fig. 2-4, and described briefly in the following paragraphs which are abstracted in part from Duntley, *et al.* (1970 and 1972).

The airborne scanner control console consists of six individual panels mounted in a standard 19 inch rack (Fig. 2-4), plus a remote start/stop function located at a nearby crew station (not illustrated). The component panels are: (1) scanner control panels, two each, (2) programmer control panel, (3) programmer panel, (4) gyro control panel, and (5) general purpose power distribution panel.

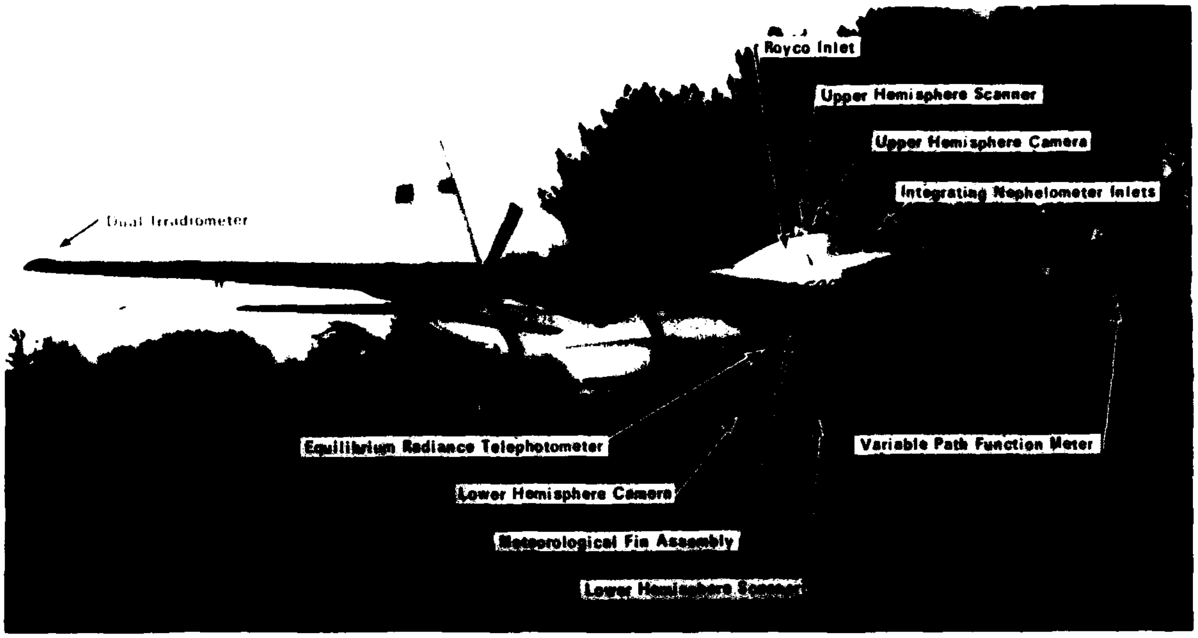

Fig. 2-1. C-130 Airborne instrument system.

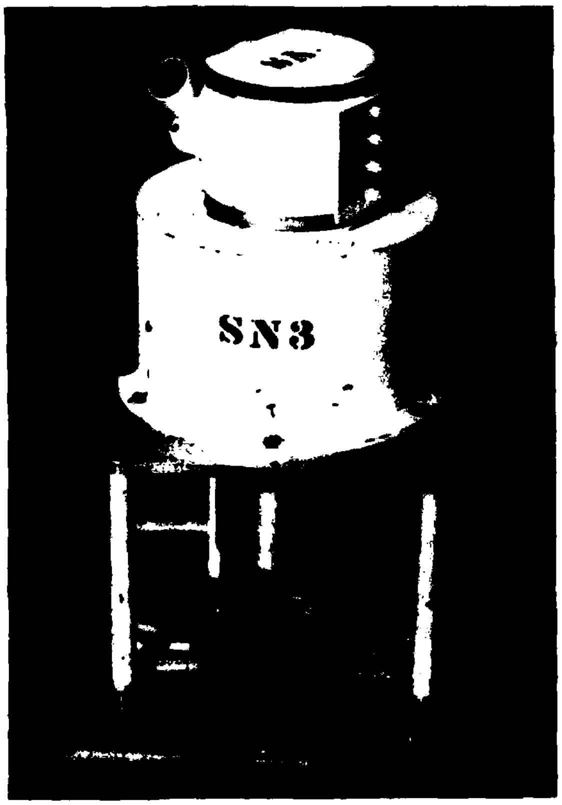

Fig. 2-2. Automatic 2π scanner assembly.

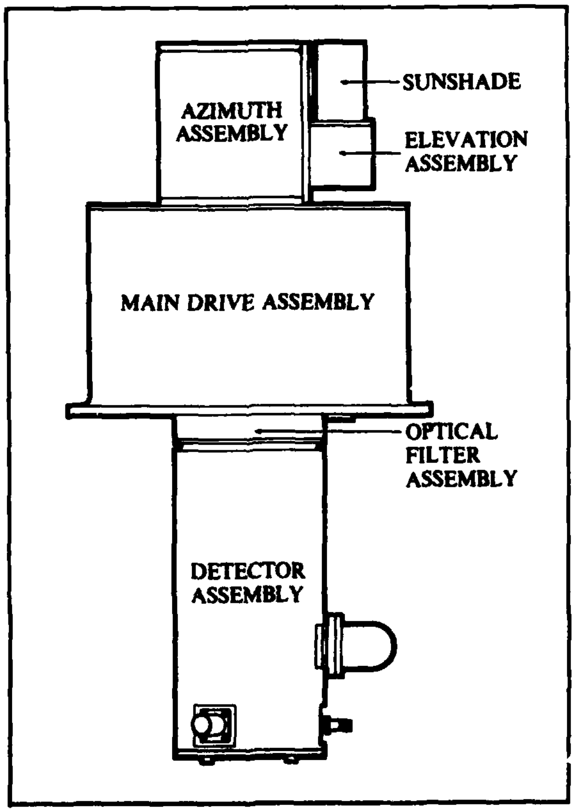

Fig. 2-3. Automatic 2π scanner outline drawing.

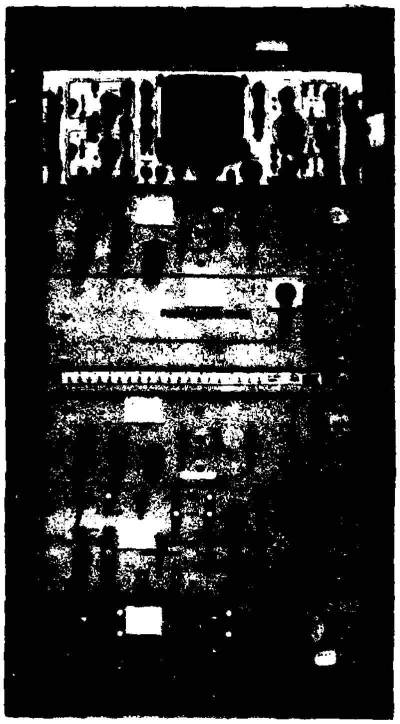

Fig. 2-4. Automatic 2π scanner control console.

Scanner Control Panels. As mentioned earlier, both the scanner azimuth and elevation drive sub-assemblies are relatively simple servo follower systems. Thus, for each scanner assembly as shown in Fig. 2-2, there is an associated scanner control panel which contains the individual demodulator, servo transmitter and drive power circuitry. Spare panels were always on-board for in-flight replacement in the event of electrical malfunction.

Programmer Control Panel. In order to direct a 2π scanner's field of view in any given direction, transmitter instructions may be generated in either of two ways: (1) manually, via graduated hand operated dials on the programmer control panel face, or (2) automatically, via the solid state control circuits located in the programmer panel. Selector switches for choosing either of these two control modes are located on the programmer control panel. Transfer of the automatic mode start/stop control to the remote panel at the crew station console is accomplished via the programmer control panel, as is synchronization of the scanner search program with the in-flight data logger.

Programmer Panel. The actual automatic pattern that the scanner field of view traverses is established by a solid state logic control array located in the programmer panel. In the early development stages of the automatic 2π scanner assembly, there was a strong demand for a flexible, high speed pattern control assembly. The most appropriate technique available at the time involved the development of an in-house design utilizing a standardized logic card and rack assembly available from Computer Control Co., Inc.

The original pattern called for a full 2π steradian search, plus reset, in 32 seconds, Duntley, *et al.* (1970). The azimuth drive was constant at one revolution per second. The elevation drive followed a variable rate ramp function. This scan rate was too fast for many applications and consequently a timing modification was inserted to slow the entire routine down to one fifth its original speed. In this slower mode the full 2π steradian search was accomplished in 160 seconds, with the azimuth sweep constant at 5 seconds per revolution.

With the advent of several data processing sophistications, it became apparent that further scan pattern alterations were necessary. Consequently, in early 1972 a major revision to programmer panels was instituted. The salient features of this modification were as follows:

A. In contrast with the scheme originally established, as in Duntley, *et al.* (1970), both airborne and ground-based programmers were converted to generate the same search pattern.

B. The primary azimuth drives were slowed to 10 seconds per revolution. On the airborne system, the rate selector switch was altered to allow the operator to select azimuth rates of either 1, 5, or 10 seconds per revolution, at his discretion.

C. The elevation drives were changed to yield a constant step of 5 degrees in elevation at the completion of each azimuth sweep. In the automatic mode, the elevation angle for the first revolution was set at 2-1/2 degrees to reduce horizon clutter induced in the 5-degree field of view.

The resultant sweep pattern, used by all automatic 2π scanners during the OPAQUE deployment series, is illustrated in Table 2.1. In this pattern, the eighteen azimuth revolutions are completed in 180 sec and the reset and stop intervals are automatically deleted from the recorded data.

Table 2.1. Automatic 2π Scanner Sweep Pattern

Azimuth Revolution No.	Constant Elevation Angle	Upper Hemisphere Zenith Angle	Lower Hemisphere Zenith Angle
1	2.5°	87.5°	92.5°
2	7.5°	82.5°	97.5°
3	12.5°	77.5°	102.5°
4	17.5°	72.5°	107.5°
5	22.5°	67.5°	112.5°
6	27.5°	62.5°	117.5°
7	32.5°	57.5°	122.5°
8	37.5°	52.5°	127.5°
9	42.5°	47.5°	132.5°
10	47.5°	42.5°	137.5°
11	52.5°	37.5°	142.5°
12	57.5°	32.5°	147.5°
13	62.5°	27.5°	152.5°
14	67.5°	22.5°	157.5°
15	72.5°	17.5°	162.5°
16	77.5°	12.5°	167.5°
17	82.5°	7.5°	172.5°
18	87.5°	2.5°	177.5°

Gyro Control Panel. All azimuth and elevation analogs generated by the 2π scanner orientation potentiometers are related to the aircraft frame. If the aircraft is flying straight and level, all scanner orientation data is relatively true. Aircraft bearing is recorded on the project data logger so that corrections can be made during data processing for bearing variations during flight. However, since no corrections are made for orientation errors induced by pitch or roll, a reliable monitoring of these maneuvers, if any, was desirable. As a result, a Sperry system SP-40 vertical gyroscope was rigidly mounted to the floor of the aircraft directly below the upper hemisphere 2π scanner. Using this gyro as a vertical reference, aircraft pitch and roll analogs were generated and fed to the in-flight data logger. The erection and control circuits required to drive and monitor the project gyro are contained in the gyro control panel.

The optical components within the scanner assembly are illustrated in Fig. 2-5 which has been compressed slightly to simplify the illustration. The flux beam emerging from the telescope's exit pupil is slightly divergent such that an image approximately 10mm in diameter is incident upon the detector's 25mm diameter photocathode. The detector assembly which has been described earlier in Duntley, *et al.* (1975), is illustrated in Figs. 2-6 and 2-7. The essential characteristics of this detector circuit are listed below.

Power Input: 28VDC at approx. 300 ma max.
Signal Output: Selectable, 0 to ±10VDC
Dynamic Range: Calibrated over 5 decade change in radiance

The output of the scanner's radiometer circuit was sampled sixty times per second by the on-board system data logger. For most applications, these constant zenith angle but azimuthally increasing data points were averaged to yield one radiance value for each six degrees change in azimuth. Thus the sky or terrain radiances measured by this system normally ended up in a 60x18 data array wherein the 2π steradians were represented by an average radiance value every six degrees in azimuth and every five degrees in elevation (*i.e.* zenith angle). The complete (unaveraged) data base was retained in back-up for diagnostic troubleshooting and special purpose displays.

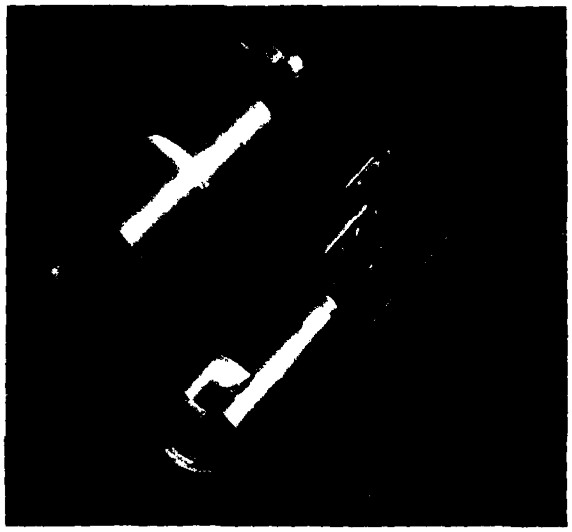

Fig. 2-6. Visibility Laboratory integrated radiation detection assembly.

The spectral characteristics of the scanner system's radiometer are illustrated in Fig. 2-8 and Table 2.2. The detector, an EMR541E series photomultiplier (S-20 spectral response) was fitted with a selection of interference and absorption filters to yield the illustrated spectral responses. The relative response labeled number 4 is similar to the photopic response of the human eye, and thus measurements made using this spectral response represent good approximations of human performance.

Some typical atmospheric properties characterizing the passbands illustrated in Fig. 2-8 are summarized in Table 2.2. The last row in Table 2.2 tabulates the appropriate properties for the true photopic response for comparison with the pseudo-photopic properties associated with response number 4. It is clear that even though responses four and nine have substantially different effective passbands, where the effective passband is the area under the normalized relative spectral response curve and is equal to the width of a rectangular passband of equivalent area, the atmospheric properties characterizing these two responses are quite similar.

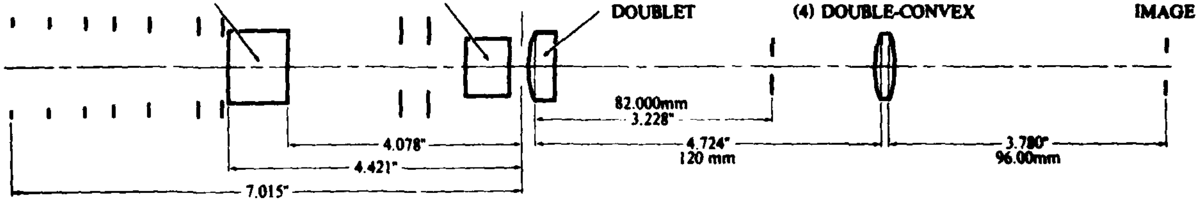

Fig. 2-5. Automatic 2π scanner optical schematic. (1) Elevation prism #396732, Jeager, 41mm x 30mm x 30mm. (2) Azimuth prism #40995, *Edmunds, 36mm x 25mm x 25mm.* (3) Achromat doublet, EFL=82, BFL=75.10, FFL=83.25, d_T=8.89. (4) Double-convex, EFL=53.64, BFL=52.04, FFL=52.00, d_T=5.91.

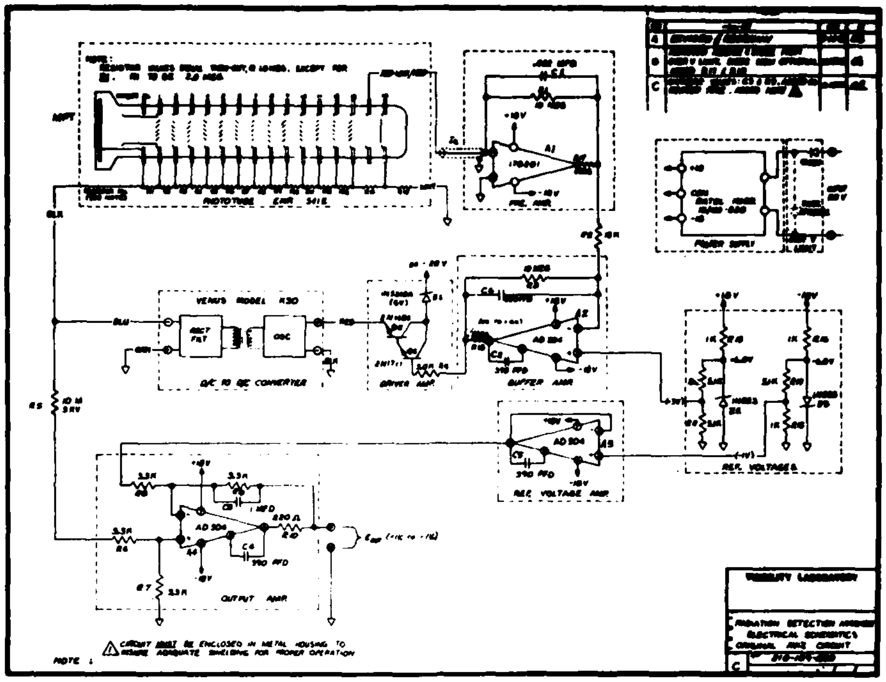

Fig. 2-7. Visibility Laboratory radiation detection assembly electrical schematic.

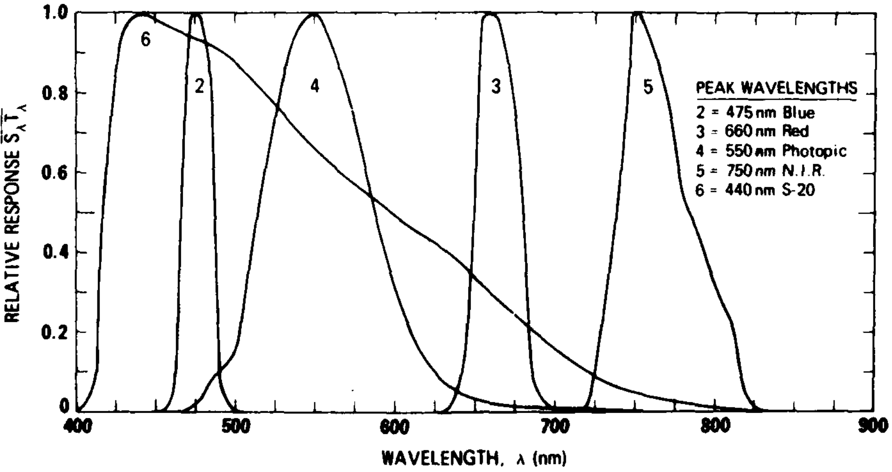

Fig. 2-8. Standard spectral responses - Project OPAQUE.

Table 2.2. Spectral Characteristics Summary for Project OPAQUE

Spectral Characteristics for Project OPAQUE				Inherent Sun Properties [Johnson (1954)]			Rayleigh Atmosphere Properties (15°C)		
Filter Code No.	Peak Wavelength (nm)	Mean Wavelength (nm)	Effective Passband	Irradiance ($w/m^2\mu m$)	Radiance ($w/\Omega m^2 \mu m$) Average	Radiance ($w/\Omega m^2 \mu m$) Center	Attenuation Length (m)	Total Scattering Coefficient (per m)	Vertical Beam Transmittance
2	475	478	19.9	2.14E+03	3.13E+07	4.07E+07	4.84E+04	2.07E-05	0.839
3	660	664	30.2	1.57E+03	2.30E+07	2.75E+07	1.86E+05	5.41E-06	0.955
4	550	557	78.5	1.90E+03	2.78E+07	3.47E+07	8.93E+04	1.15E-05	0.907
5	750	765	50.4	1.23E+03	1.80E+07	2.10E+07	3.28E+05	3.08E-06	0.974
6	440	532	183.5	1.91E+03	2.80E+07	3.55E+07	7.22E+04	1.64E-05	0.867
9	555	560	106.9	1.89E+03	2.77E+07	3.45E+07	9.22E+04	1.15E-05	0.907

3. SKY & TERRAIN RADIANCE DISPLAYS

Partial summaries of data availabilities, applications, and selected display formats related to the airborne measurements conducted with the C-130 mounted system have been presented previously in each of the technical reports listed in Appendix C. The most comprehensive of these earlier reports is presented by Duntley, *et al.* (1978c). For the majority of cases, however, these summaries addressed data other than the specific radiance arrays produced by the Automatic 2π Scanner Systems. Therefore, in the following sections of this current report we will address specifically the sky and terrain radiance measurements collected during a series of European flights conducted in conjunction with program OPAQUE, Fenn (1978) and Johnson, *et al.* (1979).

As noted in Duntley, *et al.* (1978c), there were nearly ninety separate flights conducted during the five different OPAQUE deployments. Many of these flights were made under poor weather conditions which resulted in only partial completion of the anticipated flight profile. Thus, not every flight would yield sky and terrain radiance measurements, even though there were measurements of volume scattering coefficient profiles. A summary of the number of flights yielding each of the two basic classes of data *i.e.* 1) sky and terrain radiances, and 2) scattering coefficient profiles, is shown in Table 3.1.

Table 3.1. Summary of OPAQUE Data Attempts

Deployment	Number of Flights			
	Sky & Terrain Radiance	Scattering Coefficient Profiles Only	Aborts	Totals
OPAQUE I	9	0	4	13
OPAQUE II	9	4	0	13
OPAQUE III	9	3	1	13
OPAQUE IV	14	13	2	29
OPAQUE V	16	3	1	20
Totals	57	23	8	88

As of September 1981, there were 42 successful and 5 partially successful recoveries of sky and terrain radiance sets, where a "successful recovery" is defined as a flight yielding a full array in at least two spectral bands at two or more different altitudes, a single (2+2) profile in the notation of Duntley, *et al.* (1978c). Lists of these recovered data are tabulated in several convenient formats in Section 4. The ten flights for which sky and terrain radiances were measured, but for which no data were recovered are documented on data tapes containing severe parity error problems which preclude their immediate processing. The displays presented in the remainder of this report are typical of those available from the successfully recovered data arrays.

The optimum set of sky and terrain measurements for a single flight results in a pair of data arrays representing radiance distributions as seen from each of four different altitudes and in each of four different spectral bands, a "Dual (2+4)" profile in earlier notation. Thus for each optimum flight episode, sixteen pairs of data arrays will emerge from the post flight data processing sequences. In order to cope with the analysis and evaluation of these data, several different graphical formats have been developed, which are illustrated in Figs. 3-2, 3-3 and 3-4. Each of these displays may be derived from the same basic tabular array which contains a radiance value at every six degrees in azimuth and five degrees in zenith angle. It is possible however, to retrieve the data at smaller azimuth intervals with special handling.

As an aid to the interpretation of radiance distributions illustrated in Figs. 3-2, 3-3 and 3-4, a pictorial representation of the measurement field is shown in Fig. 3-1. This artist's conception of the 4π radiance field which surrounded the aircraft is annotated with the angular notations and terminologies used to define the data displays which follow.

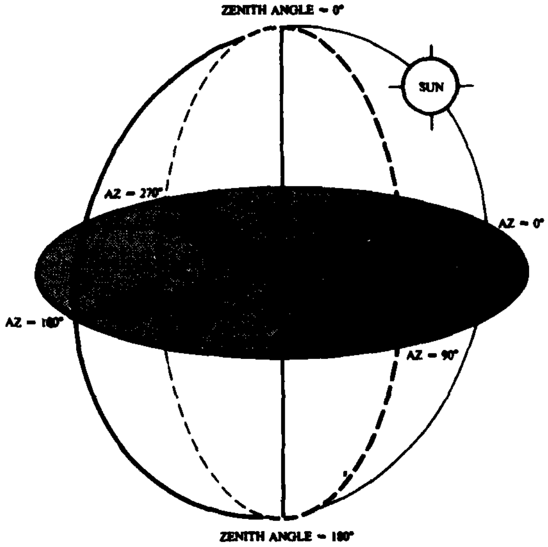

Fig. 3-1. Sky and terrain coordinate system.

3.1 Four Quadrant - Constant Azimuth Plots

The Four Quadrant - Constant Azimuth plots illustrated in Fig. 3-2 are the basic diagnostic displays used in the evaluation of the Automatic 2π Scanner data. In each plot of this type, the azimuth coordinates have been adjusted to index relative to the sun position at the time of the measurement. Thus, the data points coded as azimuth zero all were measured as the Scanner's rotating field of view intercepted the vertical sun-zenith plane, looking toward the sun. Conversely, the data points coded as azimuth 180°, were all measured as the field of view intercepted the same plane looking directly away from the sun. The two sets of points coded azimuth 90° and 270° similarly represent the measurements in the two cross-sun directions. In all cases, a zenith angle of zero specifies the point in the sky directly overhead, a zenith angle of 90° represents the horizon, and a zenith angle of 180° represents the point on the terrain directly below.

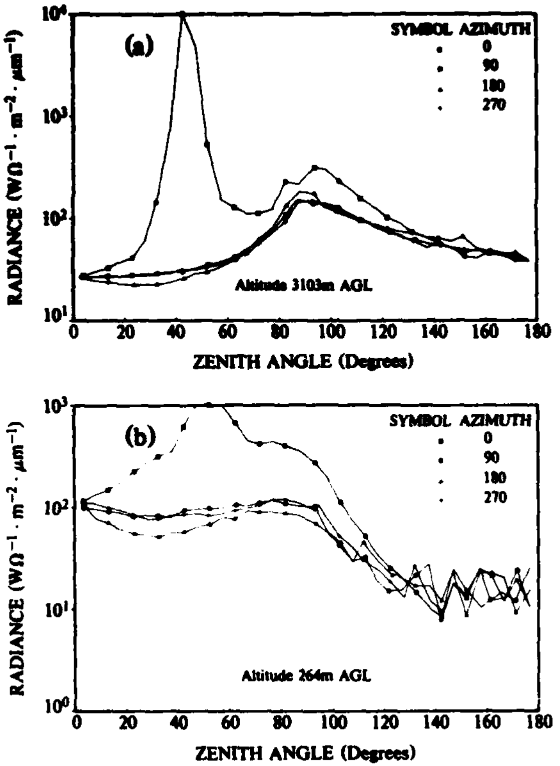

Fig. 3-2. Four Quadrant - constant azimuth radiance scans from *filter 2 of Flight C-468.*

The two sets of curves in Fig. 3-2 illustrate several major atmospheric characteristics one consistently observes in analyzing data of this sort, and in relating the measurements to the visually observed world.

a. The sky radiances are orderly in the magnitudes. The up-sun, azimuth zero data are the highest, the down-sun azimuth 180° the lowest, and the cross-sun, azimuths 90° and 270° fall neatly in between.

b. The sky radiances away from the sun are substantially higher at the lower altitude (264m AGL) as one would expect from the increased path radiance influence.

c. The horizon radiances are substantially higher than either the zenith or nadir radiance at the higher (3103m AGL) altitude.

d. The variations in terrain radiance are smoothed markedly as the altitude of measurement changes from 264 to 3103m AGL.

e. The high radiances near the sun drive the radiometer offscale, and the measurements show evidences of being adversely influenced by stray light within the optical system.

3.2 Solar Almucantar Plots

A special set of measurements were normally included in each Automatic 2π Scanner sequence in an attempt to more fully document the radiances in the near vicinity of the sun. This measurement sequence referred to as the SUN MODE sequence, involved a rescan of three selected azimuth revolutions after first inserting a 3 log neutral density filter into the scanners optical path. The insertion of this filter prevented the near-sun radiances from saturating the radiometer circuit and permitted the measurements *illustrated in the top graph of Fig. 3-3.*

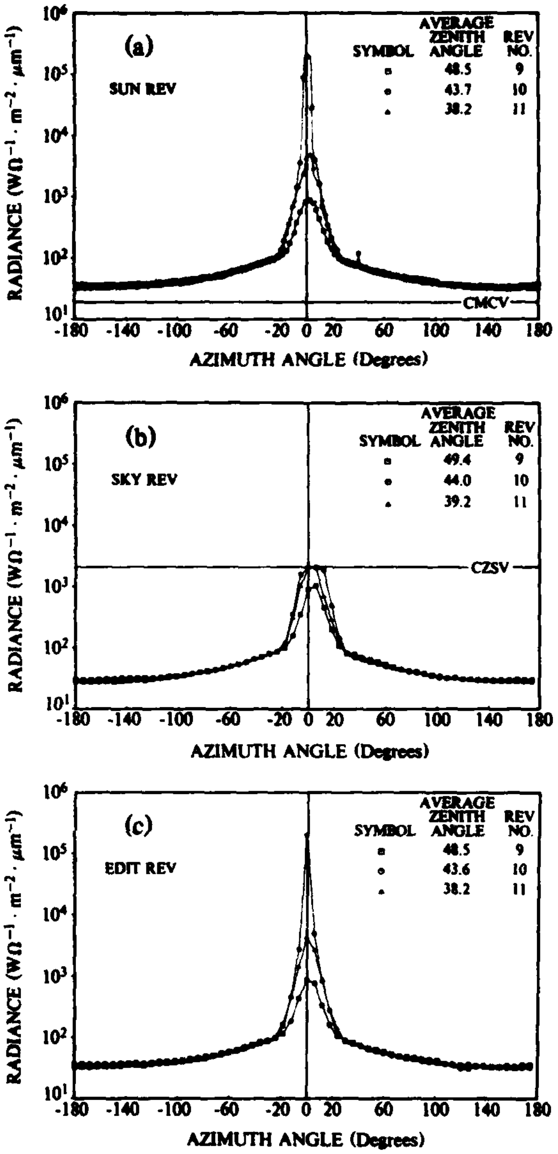

Fig. 3-3. Solar almucantar scans, direct and composite. Flight C-468, filter 2, altitude ~ 2960m AGL.

The measurements made through the neutral density filter were referred to as the SUN MODE REVOLUTIONS and their plot (3-3a) is annotated SUN REV for identification. One notes from the plot that all data points

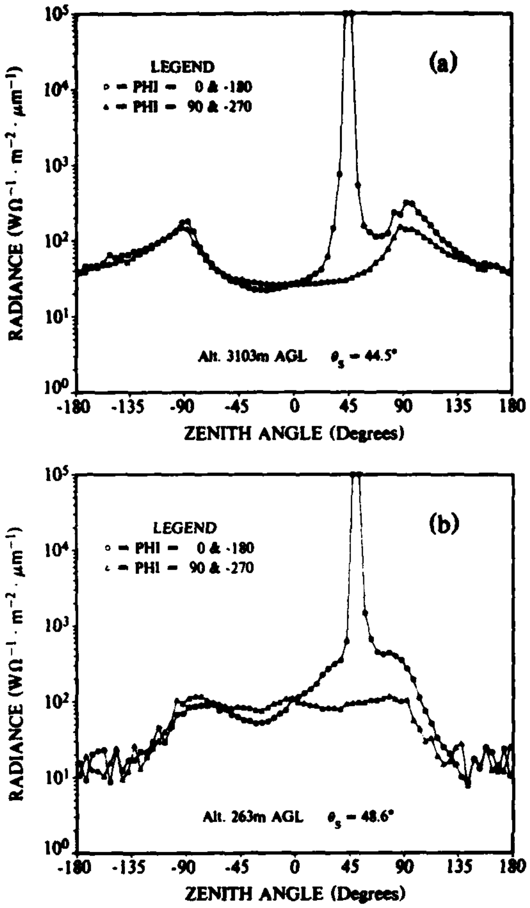

Fig. 3-4. Composite sky-terrain radiance scans. Flight C-468, filter 2.

lie above the corrected minimum calibratable value (CMCV) measurable by the 5 decade radiometer span. The "corrected minimum calibratable value" (CMCV) represents that radiance which is the minimum radiance value that the detector can usefully discriminate after being properly corrected for spectral band and sensitivity shifts. For these systems it is the radiance level at which the detector output is either three decades below the radiance established by the systems internal Isolite luminous reference cell or at which the signal to noise ratio becomes unacceptable, whichever occurs first.

Measurements made without the neutral density filter, made immediately preceding the SUN MODE, and for the same three scanner revolutions are illustrated in Fig. 3-3b and are identified as SKY REV data. These measurements, as illustrated in both Figs. 3-3b and 3-2 exceed the corrected zero scale value (CZSV) of the radiometer in the region near the sun, and thus are not reliably retrievable. The "corrected zero scale value" (CZSV) represents that radiance which is the maximum radiance value that the detector can usefully discriminate after being properly corrected for spectral band and sensitivity shifts. For these systems it is optically adjusted to be that radiance level which occurs two decades above the radiance established by the system's internal Isolite luminous reference cell. The reference radiance is established such that the system's five decade span will cover all radiance levels normally encountered during a field measurement program.

A computer generated composite of the two data sets discussed above, *i.e.* the SUN REV and SKY REV data, is illustrated in Fig. 3-3c and is identified as the EDIT REV data. In this composite set, the computer has matched those data points where the SUN REV and SKY REV values were equal after adjusting for filter offsets, and combined this matched set into a single array in which the values from the SUN REV are used in those regions where the SKY REV data were beyond the CZSV, *i.e.* exceeded the calibrated span of the radiometer. Thus, the inclusion of these EDIT REV data points in the final data array representing the measured values of sky radiance results in a single array containing a measured value for every point in the sky, including the immediate vicinity of the sun.

As with the interpretation of Fig. 3-2, there are several repeating characteristics one regularly observes when analyzing the displays of Fig. 3-3.

a. The average radiance over the scanner's five degree circular field is such that the peak values in the SUN REV are normally about 3.5 decades above the average sky radiances.

b. *Since the SUN REV displays plot data representing* the fixed azimuth scan which occurs nearest the true solar zenith angle plus data from the preceding and following scans, one may deduce the extent to which the solar disc was centered in the field of view during the nominal solar intercept. The key to this deduction is the symmetry of the before and after scans. That is, if the preceding and following almucantar scans are exactly congruent, then they were symmetrically located above and below the disc and the central scan would fully capture the disc within its field of view. There is of course, due to the 5° field of view of the instrument, a family of increasing assymetries for which the disc is still captured by the SUN REV but with decreasing certainty.

c. Comparison of these almucantar radiances with modelled aureole and surround radiances indicate the measured near-sun sky radiances may be too high.

3.3 Composite Sky-Terrain Radiance Scans

The sky and terrain radiance displays, illustrated in Fig. 3-4 are a condensed version of the Four Quadrant plot shown in the preceding Fig. 3-2, and are created from the same tabular data base. In these composite plots, the radiance variations throughout the sun-zenith plane in both the up-sun and down-sun directions are plotted as a single curve, and labeled "PHI-0 & -180°". Similarly, the data in the cross-sun plane are plotted continuously and labeled "PHI = 90 & -270°". In all cases, a zenith view angle of 0° represents the point in the sky directly overhead, and a zenith view angle of 180° represents the point on the underlying terrain directly below as illustrated in Fig. 3-1. The negative signs associated with angular indices are an artifact of the computer sorting technique, and should not be rigorously interpreted. In general, the negative sign is used merely to designate the two different azimuthal directions associated with each spherical scan.

The utility of the composite plots shown in Fig. 3-4 lies in the compact visualization of the radiance field surrounding the aircraft at the time of measurement. The radiance field characteristics discussed briefly in conjunction with the Four Quadrant displays tend to be more clearly and succinctly defined in the composite plots. Thus, visual comparisons by the analyst tend to be simpler and faster. Having the entire upper hemisphere radiance pattern presented symmetrically about the center of the plot is intuitively satisfying to most users and enhances ones association of the data display with ones concept of the real world.

4. DATA EVALUATION

The data displays illustrated in Fig. 3-4 represent the format used on all of the Automatic 2π Scanner measurements that were retrievable from the OPAQUE series of deployments. Thus a plot similar to 3-4a is available for each of a broad selection of measurement scenarios. The situations for which these sky and terrain radiance representations have been processed are summarized in Table 4.1, segregated by geographical location in Table 4.2, segregated by "number of plots per flight" in Table 4.3, and segregated by upper hemisphere cloud classification in Table 4.4. As indicated in these summarizing tables, the preponderance of the radiance data were collected over five of the OPAQUE stations: Meppen and Birkhof, Germany, Rodby, Denmark, Yeovilton, England and Bruz, France. It is also apparent that there is a good distribution of relatively complete sets *i.e.* all four spectral bands at all four altitudes (9 flights) or all four spectral bands at each of two altitudes (15 flights). Thus, with a data base of nearly 500 graphical displays, one may confidently address the use of these data in a variety of technical applications, dependent only upon an assessment of the reliability and quality of the measurements.

Table 4.1. Summary of Sky and Terrain Radiance Measurements

			Filter 2 Flight Altitudes (m AGL)				Available Radiance Data Spectral Bands ($\bar{\lambda}$, nm)				
FLT NO	DATE	SITE	A	B	C	D	478	664	557	765	Total Plots
	(1976)										
378	12 May	RB	282	1756	-	-	AB--	AB--	AB--	AB--	8
379	17 May	RB	304	1614	3170	6243	ABCD	ABCD	ABCD	A-C-	14
	(1976)										
390	25 Oct	RB	286	1514	3006	6079	ABCD	ABCD	ABCD	ABCD	16
392	1 Nov	MP	436	1176	-	-	AB--	AB--	AB--	AB--	8
393	2 Nov	MP	309	-	-	-	A---	----	----	----	1
394	18 Nov	RB	220	943	-	-	AB--	AB--	AB--	AB--	8
396	22 Nov	MP	313	-	-	-	A---	A---	A---	A---	4
399	3 Dec	BR	673	1592	2832	-	AB--	AB--	ABC-	ABC-	10
400	4 Dec	BR	691	-	-	-	A---	A---	----	----	2
401	5 Dec	BR	530	1024	2209	5297	ABCD	ABCD	ABCD	ABCD	16
402	6 Dec	BR	642	1585	-	4050	AB-D	AB-D	AB-D	AB-D	12
	(1977)										
410	4 Jul	BR	394	1615	3181	-	ABC-	-BC-	ABC-	ABC-	11
411	6 Jul	BR	421	1633	2878	-	ABC-	ABC-	ABC-	ABC-	12
412	7 Jul	BR	353	1650	2873	-	ABC-	ABC-	----	----	6
415	29 Jul	MP	218	848	-	-	AB--	AB--	AB--	AB--	8
416	1 Aug	RB	281	1549	3086	4579	ABCD	-BCD	ABC-	ABC-	13
419	4 Aug	MP	245	743	-	-	AB--	AB--	AB--	AB--	8
421	10 Aug	RB	283	1564	3394	5843	ABCD	ABCD	ABCD	ABCD	16
422	11 Aug	RB	333	1569	-	-	AB--	AB--	AB--	AB--	8

BK - Birkhof, Germany
BR - Bruz, France
ML - Mildenhall, England
MP - Meppen, Germany
RB - Rodby, Denmark
SG - Sigonella, Sicily
SO - Soesterberg, Netherlands
TR - Trapani, Sicily
YO - Yeovilton, England

Note: The nominal flight altitudes listed in columns 4 through 7, *i.e.* the altitudes associated with each of the filter 2 measurements, are coded in columns 8 through 11 to designate those altitudes at which additional spectral data are available. Thus for flight 378, the entries "AB--" in columns 8 through 11 indicate that measurements in each of the four spectral band were made at each of two flight altitudes, A=282m and B=1756m.

Table 4.1. (Cont) Summary of Sky and Terrain Radiance Measurements

FLT NO	DATE	SITE	Filter 2 Flight Altitudes (m AGL)				Available Radiance Data Spectral Bands ($\bar{\lambda}$, nm)				Total Plots
			A	B	C	D	478	664	557	765	
	(1978)										
431	1 Feb	TR	271	1503	3056	-	ABC-	AB--	----	----	5
434	18 Feb	SG	295	1602	3109	6112	ABCD	ABCD	ABCD	AB-D	15
435	23 Feb	BK	466	2284	-	-	AB--	AB--	AB--	-B--	7
436	23 Feb	BK	435	2099	-	-	AB--	AB--	AB--	AB--	8
437	27 Feb	BK	509	1538	3087	5155	ABCD	ABCD	ABCD	ABCD	16
438	1 Mar	BK	458	1619	-	-	AB--	AB--	----	----	4
439	1 Mar	BK	523	1621	-	-	AB--	AB--	AB--	AB--	8
440	2 Mar	BK	517	1664	2877	4095	ABCD	ABCD	ABCD	ABCD	16
443	9 Mar	ML	299	926	-	-	AB--	AB--	AB--	AB--	8
444	11 Mar	YO	253	714	2171	-	ABC-	ABC-	ABC-	ABC-	12
446	15 Mar	YO	207	855	-	-	AB--	AB--	AB--	AB--	8
449	18 Mar	YO	257	1029	2454	4595	ABCD	ABCD	A---	A---	10
450B	22 Mar	SO	312	1055	-	-	AB--	AB--	AB--	AB--	8
454	28 Mar	RB	266	1194	2694	4240	ABCD	ABCD	ABCD	ABCD	16
456A	31 Mar	RB	294	886	-	-	AB--	AB--	AB--	AB--	8
462	5 Aug	TR	269	1791	3730	6146	ABCD	AB-D	ABCD	-BCD	14
463	7 Aug	TR	276	1819	3674	6083	ABC-	ABCD	ABCD	ABCD	15
465	14 Aug	MP	254	1460	-	-	AB--	AB--	AB--	AB--	8
466	15 Aug	MP	202	1158	2953	6005	ABCD	ABCD	ABCD	ABC-	15
467	18 Aug	SO	250	698	2284	4717	ABCD	ABC-	-BCD	-BCD	13
468	21 Aug	MP	263	1349	3103	5850	ABC-	ABCD	ABCD	ABCD	15
469	22 Aug	SO	277	747	2475	5838	ABCD	ABCD	ABCD	ABCD	16
471	11 Sep	BK	45	535	-	-	AB--	AB--	AB--	AB--	8
473	11 Sep	BK	277	852	-	-	AB--	AB--	AB--	AB--	8
475	15 Sep	YO	325	933	3070	6135	ABCD	ABCD	AB--	ABC-	13
476	16 Sep	YO	324	1008	3085	6150	ABCD	ABCD	ABCD	ABCD	16
477	18 Sep	YO	310	623	3481	-	ABC-	ABC-	ABC-	ABC-	12
479	26 Sep	RB	307	878	2437	4620	ABCD	ABCD	ABCD	ABCD	16

BK - Birkhof, Germany
BR - Bruz, France
ML - Mildenhall, England
MP - Meppen, Germany
RB - Rodby, Denmark
SG - Sigonella, Sicily
SO - Soesterberg, Netherlands
TR - Trapani, Sicily
YO - Yeovilton, England

Note: The nominal flight altitudes listed in columns 4 through 7, *i.e.* the altitudes associated with each of the filter 2 measurements, are coded in columns 8 through 11 to designate those altitudes at which additional spectral data are available. Thus for flight 378, the entries "AB--" in columns 8 through 11 indicate that measurements in each of the four spectral band were made at each of two flight altitudes, A=282m and B=1756m.

Table 4.3. Sky & Terrain Radiances Sorted by Total Plots Retrieved

	Number of Retrieved Plots per Flight								
	16	14	12	10	8	6	4	2	1
F	390	379	402	399	378	412	396	400	393
L	401	434	411	410	392	435	431		
I	421	462	416	449	394		438		
G	437	463	444		415				
H	440	466	467		419				
T	454	468	475		422				
	469		477		436				
N	476				439				
U	479				443				
M					446				
B					450B				
E					456B				
R					465				
					471				
					473				
FLTS	9	6	7	3	15	2	3	1	1
PLOTS	144	88	87	31	120	13	13	2	1

Note: "Number retrieved" is rounded down to the nearest even number, thus those flights listed under "12" for example may yield either 12 or 13 plots. Total number of flights is 47, and the total number of plots is 499.

Table 4.2. Sky & Terrain Radiances Sorted by Site

	Flight Track Location								
	MP	RB	BK	YO	BR	TR	SO	ML	SG
F		378	435		399	431	450B	443	434
L		379	436	444	400	462	467		
I	392	390	437	446	401	463	469		
G		394							
H	393	416	438	449	402				
T	396								
	415	421	439	475	410				
N	419	422	440	476	411				
U	465	454	471	477	412				
M	466	456A	473						
B	468	479							
E									
R									
Total Flights	8	10	8	6	7	3	3	1	1

See Table 4.1 for location code.

Table 4.4. Retrieved Flights Sorted by Upper Hemisphere Cloud Classification

	Estimated Cloud Classification				OPAQUE Deployment
	Clear	Scattered	Broken	Overcast	
FLIGHT NUMBER & TYPE	379 D(2+4)			378 D(2+2)	I (2)
		390 D(2+4) 401 D(2+4)	400 D(2+4) 402 D(2+3)	392 D(2+2) 393 D(2+2) 394 D(2+2) 396 S(1+1) 399 D(2+4)	II (9)
		412 D(2+4) 416 D(2+4) 419 D(2+2) 421 D(2+4)	410 D(2+3) 411 D(2+3)	415 D(2+2) 422 D(2+2)	III (8)
		434 D(2+4) 449 D(2+4)	431 D(2+3) 437 D(2+4) 439 D(2+2) 454 D(2+4)	435 D(2+2) 436 D(2+2) 438 S(1+2) 440 D(2+4) 443 D(2+2) 444 D(2+3) 446 D(2+2) 450B D(2+2) 456A D(2+2)	IV (15)
	462 D(2+4)	463 D(2+4) 466 D(2+4) 467 D(2+4) 468 D(2+4) 469 D(2+4) 476 D(2+4) 477 D(2+3)	473 D(2+2) 475 D(2+4) 479 D(2+4)	465 D(2+3) 471 D(2+2)	V (13)
Totals	2	15	11	19	47

Note 1: The cloud classification data listed in Table 4.4 have been extracted from five previous reports related to the OPAQUE flight program, Duntley, *et al.* (1977, 1978a, 1978b) and Johnson and Gordon (1979 and 1980).

Note 2: Since many of these flights were made during rapidly changing weather conditions, substantial subjectivity is involved in the assignment of any given flight to a specific cloud condition.

Note 3: Flight type notation *i.e.* D(2+4) as indicated in previous reports is interpreted as a Dual profile each containing measurements in two spectral bands at each of four different altitudes.

4.1 Stray Light Evidences

An evaluation of the reliability of the sky and terrain radiance measurements obtained by the Automatic 2π Scanner systems has been conducted along several different avenues throughout the measurement program. In general, the directional orientation and radiometric calibration relationships have been found to be reproducible and within design specifications. *i.e.* ±0.5° in azimuth and elevation, and ±3% in absolute radiance. However, as one might suspect for an optical scanner of this design, see Fig. 2-5, there were evidences in the data indicating significant stray light influences as the systems field of view approached the location of an unobscured solar disc.

The earliest hints of potential uncertainty in the sky radiance data appeared in comparisons between values of integrated upper hemisphere scanner radiances and the dual irradiometer measurements of irradiance. These comparisons of two independently determined values of irradiance illustrated an irregular and seemingly non-systematic mismatch in the two irradiance determinations. Several possible explanations related to sampling intervals, optical averaging, and irregular cloud conditions were discussed at length, but none seemed adequate to identify the variances in the data. As a result of this uncertainty, computations of atmospheric optical properties, such as those reported in Duntley *et al.* (1976), used irradiances derived from scanner arrays as the primary data input since they were normally used in ratio form with their companion radiance data, and thus instrumental uncertainties would in most cases be minimized. However, there was a continuing concern that there was an undetected error somewhere in the experimental procedure.

With the advent of the Hering model for estimating atmospheric contrast transmittance, Hering (1981), an operationally efficient mechanism was provided for diagnostic analysis of atmospheric radiance distributions. Comparisons of sky and terrain radiance distributions calculated by the model to those measured by the airborne scanner systems are consistently excellent in all regions except near the sun. Figures 4-1 and 4-2 which have been reproduced from Hering (1981) are typical of the model-measurement comparison. It must be noted however that

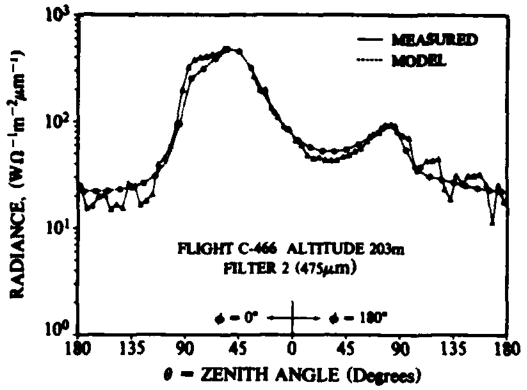

Fig. 4-1. Comparison of measured and calculated sky and terrain radiance distributions at 200m (Hering, 1981).

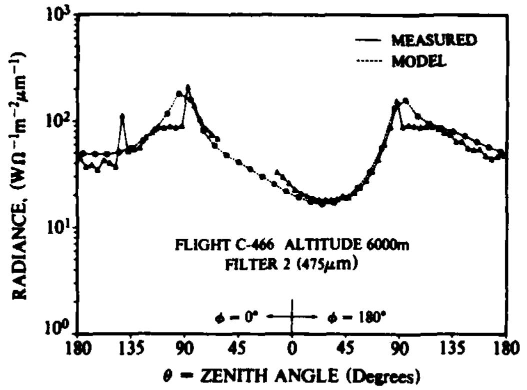

Fig. 4-2. Comparison of measured and calculated sky and terrain radiance distributions at 6000m (Hering, 1981).

the measured data in Figs. 4-1 and 4-2 have been deleted in the region near the solar zenith angle of 43°. The need for these deletions, and the source of the earlier irradiance inconsistencies were both immediately illustrated by the model comparison. When model calculations such as those shown in Fig. 4-2 were compared with sky radiance measurements as illustrated in Fig. 3-4, the near sun measurements were consistently too high with respect to the model calculation. Since modelled and measured values were consistently equivalent in all other portions of the scene, the near sun radiance measurements were considered to be the primary source of the previously unidentified experimental error.

4.2 Experimental Validation

With both irradiance measurements and model predictions indicating erroneous measurements of near sun radiances, an experimental measurement sequence was devised as a test. The procedure was straightforward. The Automatic 2π Scanner System was recalibrated and set up for operation with manual tracking control and with the radiometers sensitivity adjusted to permit direct solar viewing. The following measurement sequence was then repeated several times daily for a period of about ten days.

A. Measure apparent radiance of sky at nine positions along the solar almucantar starting at $\phi = \phi_s$ and ending at $\phi = \phi_s + 55°$, where $\phi \equiv$ azimuth angle of the center of the scanner's field of view and $\phi_s \equiv$ azimuth angle of the sun.

B. Repeat each measurement in step A with the solar disc obscured by a 4° opaque mask.

C. Compare the radiance measurements made at each angular position with and without the occulting mask to determine the off axis stray light component in each pair of measurements.

The experimental procedure outlined above verified the existence of a substantial stray light contribution to the measured signal at all angles within 30° from the sun.

The data were collected at the surface (~300ft MSL) on days with varying aerosol loads ranging from heavy haze to relatively clear.

As mentioned in step A of the procedure outlined above, measurements of almucantar radiance were made at nine angular positions with respect to the solar azimuth. They began at $\phi - \phi_s \equiv 0°$ and then advanced to 5°, 7°, 10°, 15°, 20°, 25°, 30°, and 55°. Each measurement sequence took approximately ten minutes to complete, during which there were 2 to 3 degrees change in solar azimuth. Thus, since the measurement sequence advanced in the same direction as the sun's transit, the measured radiances occurred slightly closer to the solar disc than indicated by the nominal locations indicated along the horizontal axis of Fig. 4-3. The measurements made at 0° are not illustrated since the hardware associated with the occulting procedure was inadequate to reproducibly locate a small disc accurately at the center of the scanner's field of view and thus only the unocculted measurements were obtained. One does note however, in column 5 of Table 4.5, the progressive decrease in the average field radiance at $\phi - \phi_s = 0°$ as the aerosol loading gradually increases. The 55° data are not illustrated since at this angular distance from the sun there were never any evidences of stray light, and the inclusion of the data points would needlessly expand the scale of the illustration.

Data representing the unocculted to occulted radiance ratios at each of the remaining seven almucantar positions for each of ten separate almucantar scans are plotted in Fig. 4-3. In this figure, each of the ten plots represents the magnitude of the scanner's stray light error for a different aerosol condition as noted in Table 4.5. The stray light ratios, R_{SL}, which are indicated along the vertical axis of Fig. 4-3 are defined by

$$R_{SL} = \frac{\text{Apparent Sky Radiance at } \phi_i \text{ with Scanner Aperture fully Illuminated}}{\text{Apparent Sky Radiance at } \phi_i \text{ with Scanner Aperture fully Shadowed}}$$

Table 4.5. Data Index for Straylight Measurements

Test Number	Date Oct 1980	Plot Symbol	Straylight Ratio @ 5°	Relative* Radiance @ 0°	General Remarks**
2	20	●	36.9	0.97	Thin haze
6	24	▲	34.9	1.00	Base of mountains visible @ 28mi
10	30	•	31.0	0.97	
3a	21	●	23.8	0.89	Thin cirrus
5a	23	■	21.0	0.93	Base of mountains not visible @ 28mi Bridge visible at 6mi
9	29	⊙	16.6	0.89	
7	28	+	16.1	0.93	Tijuana not visible @ 17 mi
8	29	×	11.8	0.83	
1	13	⊡	8.3	0.87	Moderate haze
4	2	●	6.4	0.64	Heavy haze bridge barely visible @ 6 mi

* Unocculted radiances normalized to maximum within the set. For general reference and alignment purposes only.

** All measurement sequences were made between 1000 hrs. and 1400 hrs. local time.

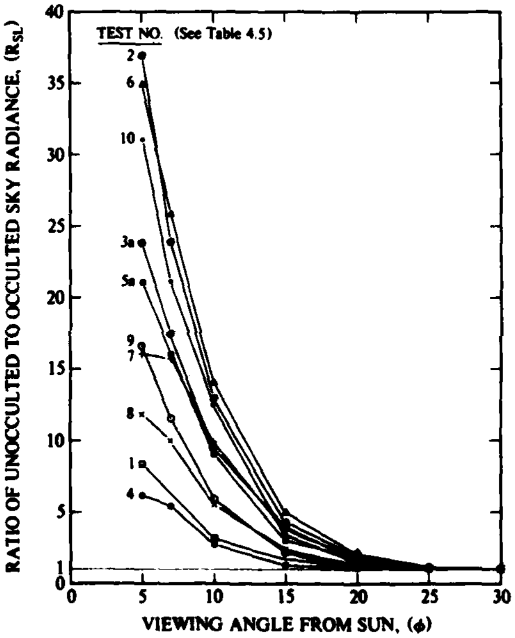

Fig. 4-3. Experimentally determined straylight effects.

where for the denominator measurement the scanner entrance aperture is centered in the shadow cast by an opaque circular disc which subtends a field of 4° as seen from the scanner entrance.

It is apparent from the data illustrated in Fig. 4-3 that the off-axis light entering the scanner's optical system is substantial at all viewing angles near the sun, and increases markedly both as the field of view approaches the solar disc and as the atmospheric aerosol loading decreases.

The influence of the aerosol load on stray light error and thus the fidelity of the scanner's radiance measurements is illustrated best perhaps by considering two contrasting examples. In both examples consider the measurement of sky radiance at the same distance from the sun, however in the first example the measurement is made with the scanner at 6 km in altitude and in the second at only 1 km.

At 6 km the aerosol loading is typically very low with atmospheric optical scattering ratios *i.e.* total scattering/Rayleigh scattering, Hering (1981), in the order of 1.2 to 1.5 whence the apparent radiance of the predominantly blue sky is relatively low. Conversely, the direct solar irradiance falling obliquely upon the scanner's entrance aperture is only slightly attenuated by its passage through the thin upper atmosphere and thus gives rise to relatively high level off-axis reflections within the optical system. These conditions would give rise to high stray light ratios, R_{SL}, such as those illustrated by the curves from tests 2, 6 and 10 shown in Fig. 4-3.

In the example with the scanner at only 1 km altitude the measurement of apparent sky radiance is made through a much more turbid medium in which the typically heavier aerosol load generates substantially higher optical scattering ratios and their resultant higher proportion of forward scattering. In this example the apparent radiance of the now hazy sky is high relative to that measured at 6 km, however the same scattering mechanism which has increased the apparent sky radiance, has also contributed to the attenuation of the direct solar irradiance falling upon the scanner's aperture and thus reduced the intensity of the system's internal stray light. This second example illustrates the mitigating influence of the aerosol loading upon the scanner measurement's stray light component. These low altitude conditions would give rise to lower stray light ratios R_{SL}, such as those illustrated by the curves from test numbers 8, 1, and 4 shown in Fig. 4-3.

In the full overcast condition, where the irradiance from a sky segment just off-axis is not substantially higher than that from an on-axis segment, or at viewing angles in excess of 30° from the solar disc there are no discernible stray light influences upon the scanner's radiance measurements and the values of R_{SL} approach one as illustrated along the lower, right hand boundary of Fig. 4-3.

The implications to be derived from these data are that high altitude or clear day measurements of sky radiances within 10° of the solar disc will have stray light ratios of as much as 20 to 35, whereas low altitude near-sun measurements through more turbid atmospheres will have substantially lower stray light ratios of about 3 to 6 at the same angular distance from the disc. In either case it is clear that with stray light influences of the magnitude illustrated in Fig. 4-3, the data displays such as Fig. 3-2a, in order to be fully reliable, should in fact be presented in a form such as that illustrated in Fig. 4-4. (Johnson and Hering 1981). Fortunately, the same model that pinpointed the erroneous measurements provides the vehicle for a *realistic* correction procedure.

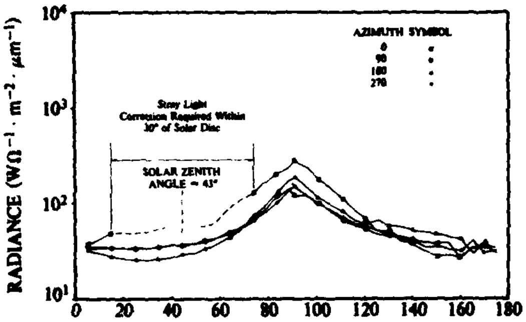

Fig.4-4. Measured sky and terrain radiance distributions for Flight C-466, filter 2, 2953m AGL.

4.3 Stray Light Corrections

Inasmuch as the data in Fig. 4-3 illustrate that the validity of near sun radiance measurements is highly influenced by the variations in atmospheric aerosol loading, the selection of an appropriate corrective procedure is somewhat limited. Only two have been considered at this point and they are described briefly in the following paragraphs.

The first procedure is to use an extrapolation from the last valid measurement nearest the sun to calculate new sky radiance values. A technique used by Barteneva (1960) to extrapolate measured directional scattering functions from 16° scattering angle to 0° scattering angle was applied to the flight C-466 sky radiance data as a test. In this technique one assumes the log of the sky radiance to be a linear function of the scattering angle cosine between 30° and 0° scattering angle. This relatively familiar relationship is expressed as an assumed equality in Eq. (4.1),

$$\ln L_\infty^*(z,\theta,\beta) = \ln A + B \, \mathrm{Cos}\beta \tag{4.1}$$

where $L_\infty^*(z,\theta,\beta)$ is the sky radiance *i.e.* upward looking path radiance, at altitude z at zenith angle θ and at scattering angle β from the sun. The technique, is reasonably effective, even though it tends to significantly underestimate the diffraction peak of the phase function as illustrated in Fig. 4-5a. Fortunately, when used to fill in near-sun sky radiance values which will be integrated in conjunction with a separate apparent solar disc radiance as discussed in Duntley, *et al.* (1975) the residual error at the total irradiance level is small. For example, when applied to the flight C-466, 478nm, high altitude data, the calculated irradiances, which had originally been as much as 14% higher than those measured by the irradiometer system, were brought to within ±4% of the measured values.

A second technique is based upon the demonstrated ability of the Hering model to recreate the measured values of the diffuse radiance field and the vertical structure of the irradiance distributions. In this procedure, the valid measurements within the array *i.e.* the radiance measurements more than 30° from the sun, in conjunction with the model algorithms, establish both the form and the magnitude of corrected radiance field. The procedural concept assumes that the single scattering phase function can be represented analytically with good precision by two term Henyey-Greenstein functions (Irvine, 1968) even though these two term functions also tend to underpredict the forward 10° of the phase function as is illustrated in Fig. 4-5b which has been adapted from Kattawar (1975), and that these analytic expressions are directly relatable to the measured optical scattering ratio. Johnson *et al.* (1979) and Hering (1981).

Even though it is more complex computationally, there are specific advantages to be gained in pursuing the further development of this second technique. Not only do the Henyey-Greenstein functions more closely approximate the forward scattering regions of the atmospheric phase function as illustrated in Fig. 4-4b, but the flexibilities inherent in conditioning the Hering model inputs to the measured environment add substantial realism to the computed radiances. As indicated in Appendix B, abstracted from Hering (1981) and which summarizes the operation of his model, the model inputs are designed to take full advantage of the most descriptive data available. The key inputs are the optical scattering mixing ratio, $Q(z)$, and the single scattering albedo, $\omega(z)$, where $Q(z)$ is defined as the ratio of the total volume scattering coefficient at altitude z, to the molecular (or Rayleigh) volume scattering coefficient at the same altitude z; and $\omega(z)$ is defined as the ratio of the total volume scattering coefficient at altitude z, to the volume attenuation coefficient as determined at altitude z. The model will from these specified inputs compute the Henyey-Greenstein functions associated with the input $Q(z)$ values and proceed with the computation of sky radiance. However, to the extent that more complete information is available to define $P(z,\beta)$ the atmospheric phase function at altitude z, the model will readily accept this information in lieu of the computed values estimated from the specification of $Q(z)$.

The fidelity with which the Hering model has reproduced sky radiance measurements in regions free from stray light contamination, as illustrated in the preliminary run shown in Figs. 4-1 and 4-2, indicates the high probability that it will produce accurate estimates of the true sky

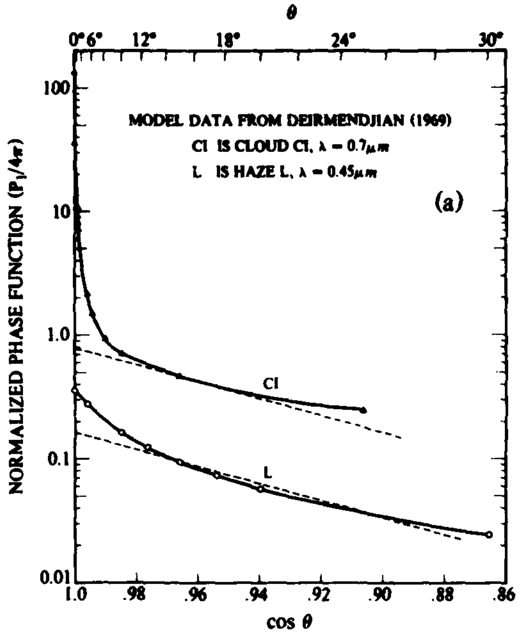

Extrapolation assuming scattering phase function linear with cosine of scattering angle.

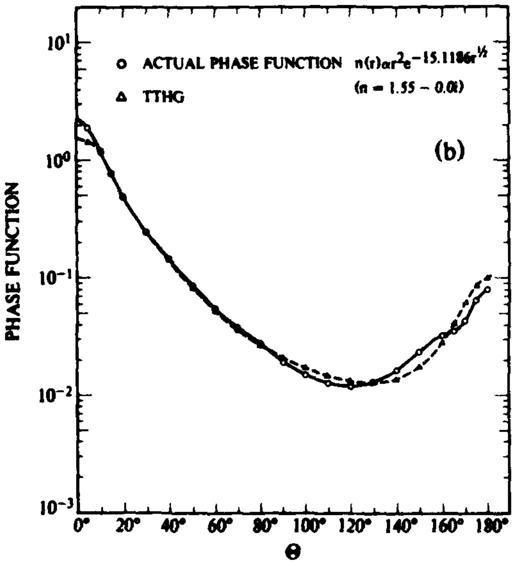

Approximation assuming scattering phase function represented by two term Henyey-Greenstein function [from Kattawar, (1975)].

Fig. 4-5. Comparison of scattering phase function approximations with modelled calculations.

radiance in most of those regions currently contaminated. Thus the proposed corrective procedure would consist of the following steps for each set of radiances one might desire. 1) From the experimental measurements, determine and enter as input the vertical profiles of $Q(z)$, $P(z,\beta)$ and $\omega(z)$ including estimates of these profiles in the relatively clear atmosphere above the highest altitude sampled by the instrumented aircraft (normally 6 km), 2) Let the model compute the sky radiances in the planes illustrated in Fig. 3-4. 3) If necessary, adjust the input parameters to insure an acceptable model fit to the measurements in the regions between 30° and 55° from the solar disc. 4) Substitute the values of sky radiance as calculated by the model into the measured array as the approximated correct values.

It is apparent that even with this technique there will be some uncertainty in the reliability of the calculated values of sky radiance as the values approach the disc, particularly as they move inside 15° where the Henyey-Greenstein functions begin to fall short of the Mie predictions. It would be a desireable facet of the experimental validation of this process to conduct a series of simultaneous measurements using the automatic 2π scanner as described in Section 2 and the 4′ field of view Contrast Reduction Meter (CRM) described in Duntley, *et al.* (1972). These CRM data would provide significantly more reliable near-sun radiance measurements, particularly in the difficult solar aureole regions *i.e.* at scattering angles between zero and about five degrees, against which both the scanner and the model performances could be judged.

5. SELECTED SAMPLE DATA

It is beyond the scope of this report to include the nearly 500 graphs and tables which represent the sky and terrain radiances retrieved from the OPAQUE flight series. It is desireable however to illustrate to a limited degree the variety of characteristics inherent within the data set. Therefore the figures contained in this section should be considered as an hors d'oeuvre is considered, with respect to that which might follow.

Three flights have been selected to provide this sample, flight C-392 from the OPAQUE II deployment during the Fall of 1976 as reported in Duntley *et al.* (1978a), flight C-410 from the OPAQUE III deployment during the Summer of 1977 as reported in Duntley *et al.* (1978b), and flight C-468 from the OPAQUE V deployment during the Summer of 1978 as reported in Johnson and Gordon (1980). As a convenience to the reader, the flight description sheets for each of these sample flights have been extracted from the parent reports and are included herein.

THE DATA PRESENTED IN THE FOLLOWING FIGURES HAVE NOT BEEN CORRECTED FOR THE NEAR SUN STRAY LIGHT EFFECTS DISCUSSED IN SECTION 4.

Flight C-392 is one of the fifteen listed in Table 4.3 as having eight retrievable data arrays. In most cases, as illustrated by flight C-392, these eight arrays represent measurements made in each of four spectral bands at two different altitudes, a dual (2+2) profile in the notation of Duntley *et al.* (1978a). The feature most noticeable in this series of displays is the intermittent appearance of the solar peak. In order to easily calculate the contrast transmittance between the two altitudes shown in Fig. 5-1a and 5-1b for example, the radiance arrays are usually assumed to represent a snapshot in time, with only altitude differences influencing the radiance distribution. As is seen, the sun obscuration is substantially different in the array representations, and thus a more difficult computational procedure would be required. The data in Fig. 5-2a and 5-2b however represent more consistent conditions with respect to solar obscuration and could be handled readily in the traditional computational scheme, Duntley *et al.* (1976).

Flight C-410 produced ten retrievable arrays, six of which are illustrated in Fig. 5-3. This series of plots represents the second half of the total data flight and is chosen to illustrate the influence of changing cloud conditions. At the beginning of the sequence, *i.e.* during the 400m AGL runs, one notes the unobscured sun in both spectral bands, plus the enhanced terrain reflectance at the Filter 5 (765nm) wavelength (Ref. Fig. 2-8). At the intermediate altitude, the sun becomes obscured at some time between the Filter 4 and the Filter 5 sequences, and by the time the top altitude runs are made, the sky is fully overcast above 3000m AGL. In all cases the relatively high terrain radiances at 765nm are readily apparent.

Flight C-468 represents a dual (2+4) mission in which all but one of the anticipated sixteen data arrays were successfully retrieved. One notes the unobscured sun occurring in each display and the dramatic change in the relationship between sky and terrain radiance levels as the altitude of measurement increases allowing the path radiance and terrain reflectance properties to assert their influence in the measurements of the lower hemisphere.

FLIGHT C-392 - 1 NOVEMBER 1976

DESCRIPTION OF FLIGHT AND WEATHER CHARACTERISTICS

Filter Ident	Data Interval			Max. Flight Altitude (m)	Average Terrain Elevation (m)
	Start (GMT)	End (GMT)	Elapsed (hrs)		
2,3	1115	1208	0.88	1410	18
4,5	1212	1253	0.68	1170	18

Filter Ident	Solar Zenith Angle		
	Initial ST&LV (degrees)	Solar Transit (degrees)	Final V-PRO (degrees)
2,3	67.6	-	68.6
4,5	68.7	-	71.0

Flight Description. Flight C-392 was an afternoon flight. Multiple cloud layers varied from broken to overcast. The approximate northeast to southwest Meppen track was located between Oldenburg and Lathen in northwestern Germany. Typical terrain features were heavily cultivated low lying flat farmlands interspersed with occasional dark woods and small towns.

In-Flight Notes. The in-flight observer reported scattered clouds at 1500 meters (5000 feet), 7/8 altocumulus at 5400 meters (18,000 feet), 7/8 cirrus at 6000 meters (20,000 feet). By 1245 GMT the lower clouds were scattered to broken at 2100 meters (7000 feet), the altocumulus was unchanged and the cirrus had increased to overcast. Conditions worsened at the east end with the lower broken layer having tops of 2400 meters (8000 feet) and increasing to overcast by 1312 GMT. Moderate haze was observed throughout the track and the period.

Local Weather Notes. Twente, west of the track, reported 1/8 stratocumulus at 1500 meters (5000 feet) and 7/8 altocumulus at 2400 meters (8000 feet) at 1000 and 1100 GMT. The stratocumulus lowered to 750 meters (2500 feet) by 1200 GMT and the altocumulus raised to 3600 meters (12,000 feet). By 1229 GMT the stratocumulus increased to 6/8 coverage at 630 meters (2100 feet) and gradually lowered to 540 meters (1800 feet) by 1400 GMT. The altocumulus layer increased to overcast and gradually lowered to 2700 meters (9000 feet) through the afternoon. Visibility was 6 to 8 kilometers in haze.

Lingen, south of the track, reported 5/8 stratocumulus at 1200 meters (4000 feet) and 6/8 altocumulus at 2700 meters (9000 feet) with visibility 4.2 kilometers in light fog at 1100 GMT. Conditions improved to 3/8 cumulus and stratocumulus at 450 meters (1500 feet), 5/8 altocumulus at 3000 meters (10,000 feet), visibility 7 to 8 kilometers in haze. At 1500 GMT there was 5/8 stratocumulus at 750 meters (2500 feet), overcast altocumulus at 2700 meters (9000 feet) and visibility 10 kilometers.

Oldenburg and Ahlhorn, east of the track, include ceiling and visibility data in their reports but no cloud types or amounts. At Oldenburg the ceilings were reported from 1200 to 1500 meters (4000 to 5000 feet) and visibility 5 to 7 kilometers with haze. Ahlhorn reported ceilings 1500 to 2700 meters (5000 to 9000 feet) and visibility 6 to 7 kilometers in haze.

The radiosonde station at Rheine/Waldhugel was approximately 81 kilometers south of the flight track center point, but no data were taken on this date.

Synoptic Remarks. The surface chart for 1200 GMT had a weak ridge with its axis through eastern Germany. From a 960-millibar low centered south of Iceland an occlusion extended east and south-southeast through the western part of the North Sea then as a cold front south and south-southwest through western France and northwestern Spain and Portugal into the Atlantic. At 500 millibars there was a low over western Finland. A weak gradient prevailed over western Europe with light to moderate westerly winds. The airmass was stable maritime polar.

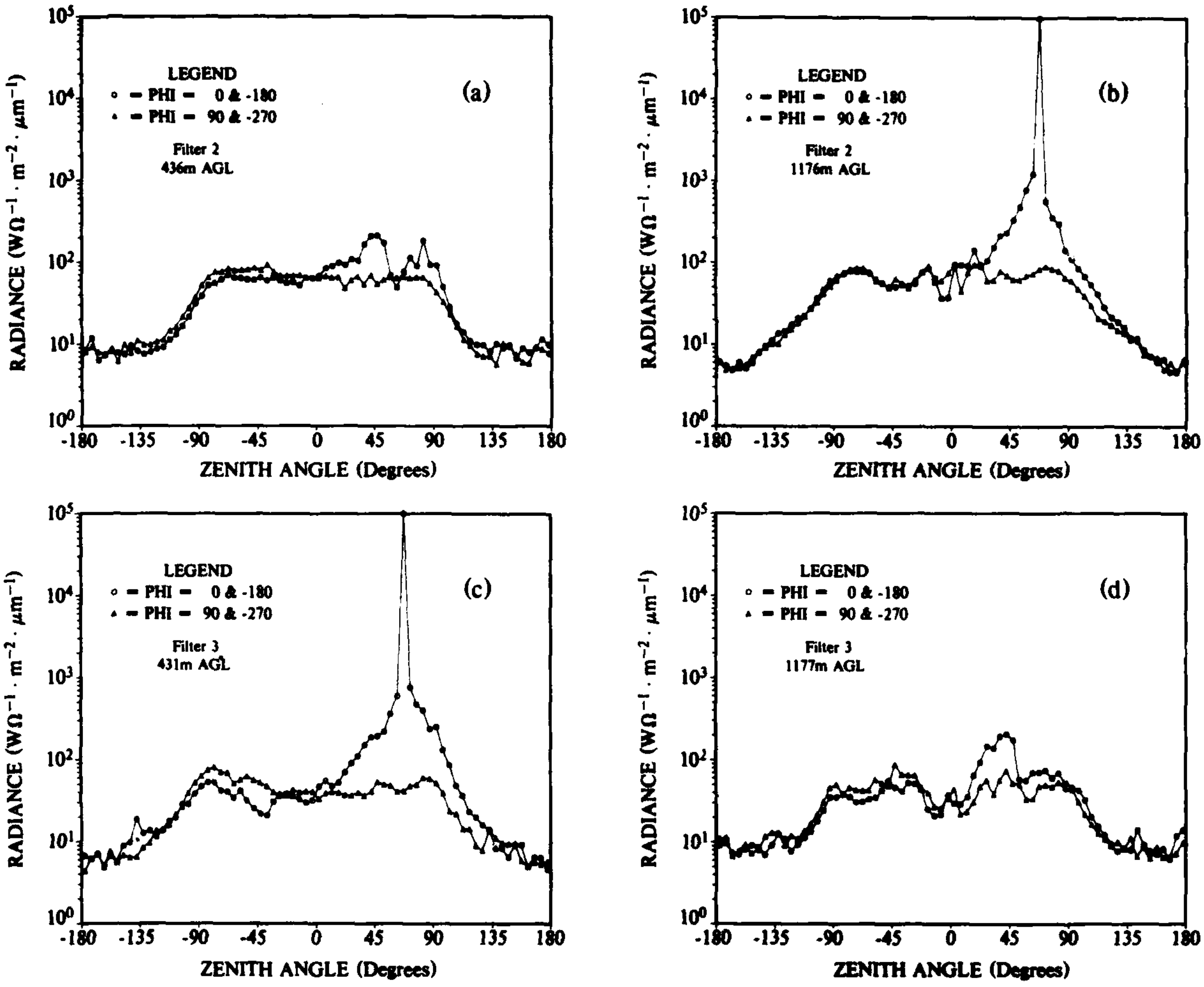

Fig. 5-1. Sky and terrain radiances - Meppen, Germany. Flight C-392, $\bar{\lambda}$ = 478nm and 664nm, θ_s = 68°.

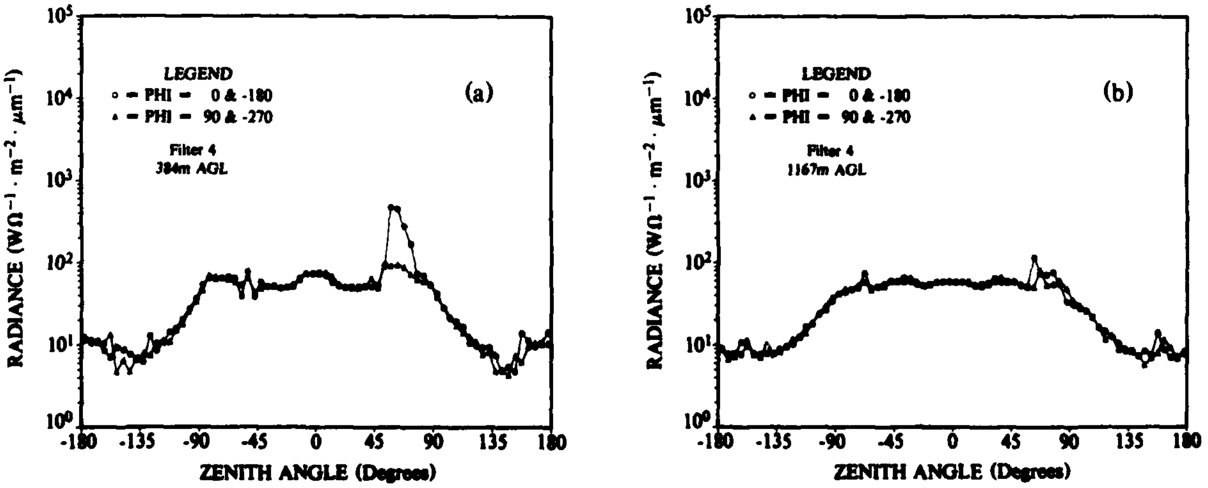

Fig. 5-2. Sky and terrain radiances - Meppen, Germany. Flight C-392, $\bar{\lambda}$ = 557nm and 765nm, θ_s = 70°.

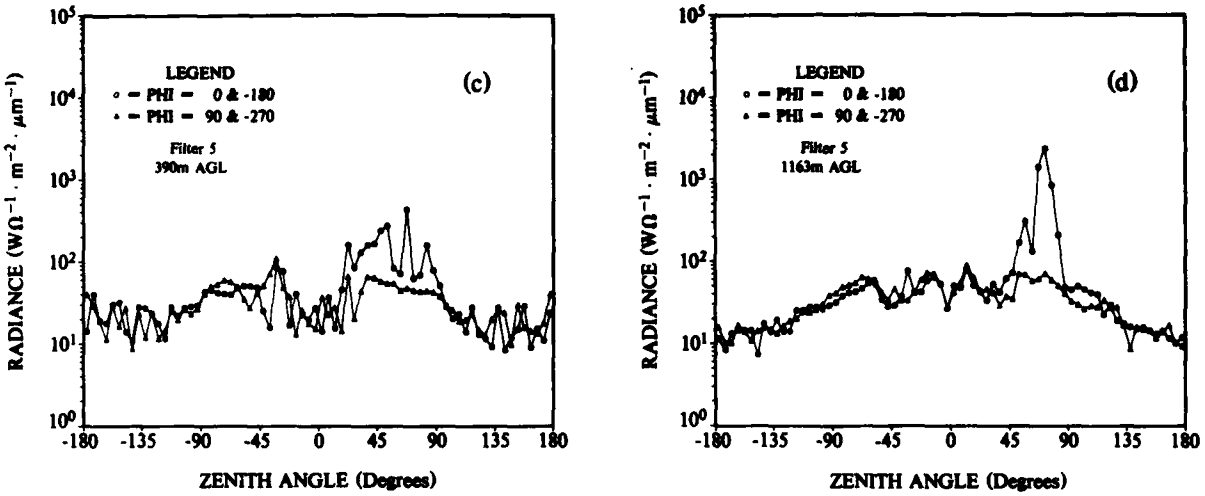

Fig. 5-2 (con't). Sky and terrain radiances - Meppen, Germany. Flight C-392, $\bar{\lambda}$ = 557nm and 765nm, θ_s = 70°.

FLIGHT C-410 - 4 JULY 1977
DESCRIPTION OF FLIGHT & WEATHER CHARACTERISTICS

Filter Ident	Data Interval			Max. Flight Altitude (m)	Average Terrain Elevation (m)
	Start (GMT)	End (GMT)	Elapsed (hrs)		
2,3	1119	1249	1.5	3180	46
4,5	1255	1432	1.6	3180	46

Filter Ident	Solar Zenith Angle		
	Initial ST&LV (degrees)	Solar Transit (degrees)	Final V-PRO (degrees)
2,3	27.2	25.2	26.3
4,5	26.6	·	37.8

Flight Description. Flight C-410 was a midday flight, spanning local apparent noon. There were multiple cloud layers varying from scattered cumulus to overcast cirrus. The approximate east-west Bruz track was centered south of Rennes in northwestern France. Typical terrain features were green and brown fields interspersed with small towns.

In-Flight Notes. The in-flight observer reported broken to overcast altostratus clouds at the beginning of the flight with scattered cumulus forming at 1200 meters (4000 feet) after 1153 GMT. Tops of the cumulus were 1500 meters (5000 feet) and built to 1800 meters (6000 feet) before the end of the flight. Moderate haze was reported at all altitudes.

Local Weather Notes. Data from Rennes, 7 kilometers north of the center of the flight track, show 1/8 to 3/8 cumulus at altitudes varying from 900 to 1380 meters (3000 to 4600 feet), 3/8 to 5/8 altostratus at 3000 meters (10,000 feet) and 7/8 cirrus at 6000 meters (20,000 feet). Visibility of 20.0 kilometers decreased to 11.2 kilometers by the end of the flight.

Nantes/Chateau Bougon, 78 kilometers south of the track center point, reported 1/8 cumulus increasing to 4/8 at altitudes varying from 1200 to 1380 meters (4000 to 4600 feet) and 3/8 to 7/8 altocumulus at 3000 meters (10,000 feet). Visibility varied from 25.0 to 11.2 kilometers.

The radiosonde station at Brest was 208 kilometers westnorthwest of the flight track center and located in a prevailing airflow that was parallel with the track.

Synoptic Remarks. The surface charts show a 1024 millibar high east of Denmark. Most of France was in a col with pressures about 1014 millibars. At 500 millibars there was a low pressure trough over southern France. The flow was easterly and the air mass was modified unstable maritime polar.

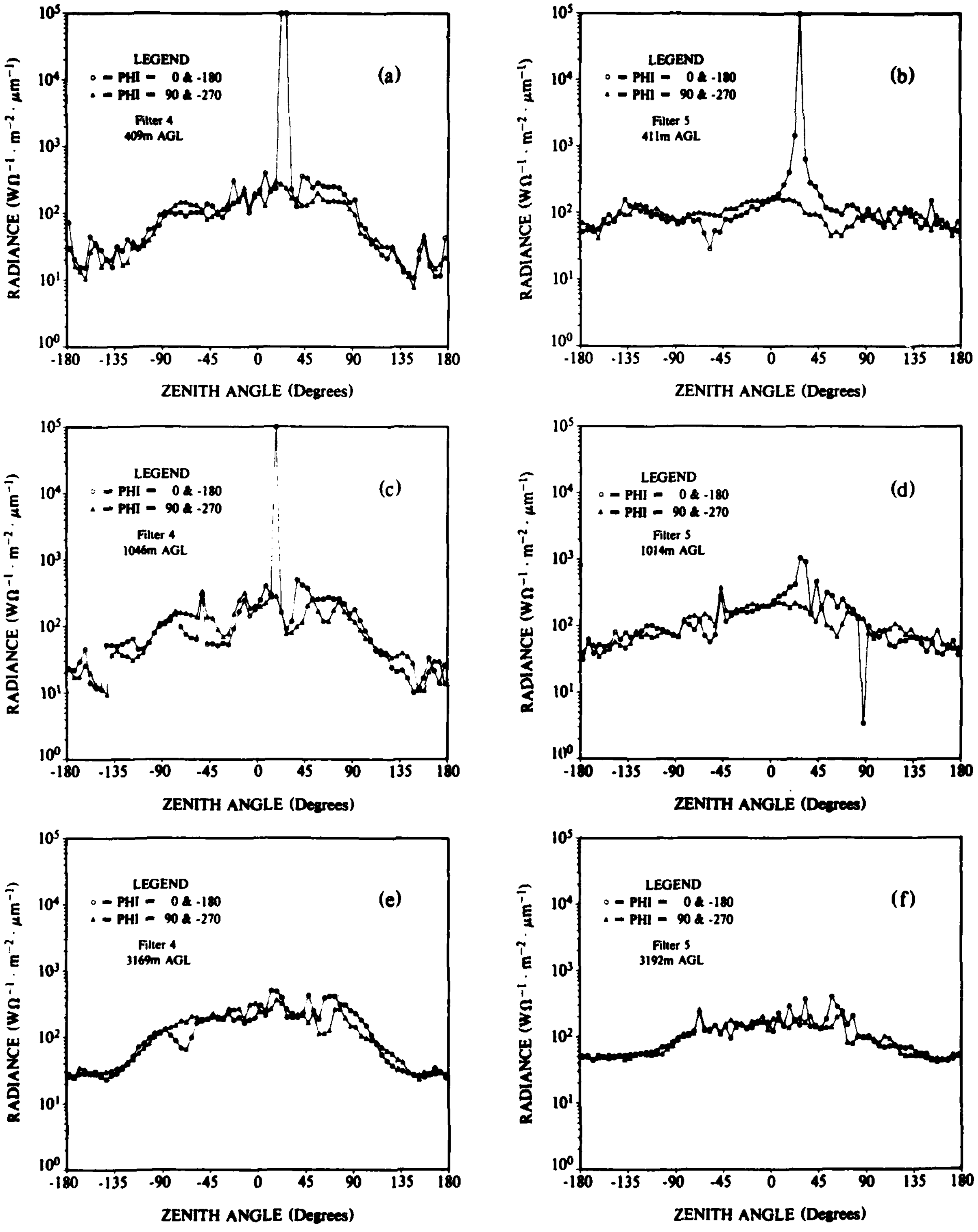

Fig. 5-3. Sky and terrain radiances - Bruz, France. Flight C-410, $\bar{\lambda}$ = 557nm and 765nm, $\theta_s \sim 30°$.

FLIGHT C-468 - 21 AUGUST 1978
DESCRIPTION OF FLIGHT & WEATHER CHARACTERISTICS

Filter Ident	Data Interval			Max. Flight Altitude (m)	Average Terrain Elevation (m)
	Start (GMT)	End (GMT)	Elapsed (hrs)		
2,3	0920	1058	1.63	5820	18
4,5	1102	1244	1.70	6210	18

Filter Ident	Solar Zenith Angle		
	Initial ST&LV (degrees)	Solar Transit (degrees)	Final V-PRO (degrees)
2,3	48.6	-	41.4
4,5	41.3	40.9	43.3

Flight Description. Flight C-468 was a midday flight spanning local apparent noon with take off at 0847 and landing at 1320 GMT. There were scattered high thin cirrus clouds. The approximate northeast to southwest Meppen track was located between Oldenburg and Lathen in northwestern Germany. Typical terrain features were green and brown fields interspersed with occasional dark woods and small towns.

In-Flight Notes. The in-flight observer noted that there was very muted horizontal banding in haze and cirrus above - gradual clearing of haze left relatively clear cirrus layers against blue sky. A weak frontal passage last night has left cirrus. A new frontal system to the northwest is causing more cirrus to move in from the northwest slowly. At 0920 GMT at 300 meters (1000 feet) there was scattered cirrus at 6000 meters (20,000 feet) with 8 kilometers (5 miles) slant range down sun. On the climb from 1350 to 3000 meters (4500 to 10,000 feet) the low altitude haze top was 1860 meters (6200 feet) with a thin clearer layer and lighter haze above. Distinct haze top of all haze at 2400 meters (8000 feet). Areas of clouds are visible to the north and south. At 1005 GMT at 3000 meters (10,000 feet) scattered cirrus at 6000 meters (20,000 feet) with scattered cumulus far to north, light haze with slant range 16 kilometers (10 miles). Cirrus appears to come down to 3600 to 4500 meters (12,000 to 15,000 feet) in places. On the climb to 6000 meters (20,000 feet) some cirrus trails were heavy to below 4500 meters (15,000 feet); cirrus are in bands with 20 to 30 nautical mile separation. Other cirrus extend up to 10500 meters (35,000 feet); basic layer is at 6000 meters (20,000 feet). At 1130 GMT at 1350 meters (4500 feet) there was scattered altostratus at 1500 meters (5000 feet) and scattered cirrus at 9000 meters (30,000 feet) with moderate to heavy haze and slant range 6.4 to 8 kilometers (4 to 5 miles). At 1145 GMT on the climb to 3000 meters (10,000 feet) it was noted that cumulus were beginning. Cirrus was present during the first half with a moderate wall to the south. A new band or cirrus was moving in from the north at a higher altitude than previously. The cumulus tended to blend into bright haze in the up sun direction. On the final descent the cumulus field was developing further along and to the south of the west end of the track. Cumulus tops were 2700 meters (9000 feet) and the haze top was now closer to 2100 meters (7000 feet). Visibility at the top of the haze layer was very poor. Visibility below 2700 meters (3000 feet) seems lower than previous.

Local Weather Notes. Bremerhaven, 87.1 kilometers northeast of track center, reported scattered high thin cirrus clouds becoming broken at 6900 meters (23,000 feet) by 1300 GMT. Visibility of 5 kilometers in haze improved to 9 kilometers by 1300 GMT.

Emden, 45.7 kilometers northwest of the track center, recorded 1/8 to 2/8 high thin cirrus becoming 5/8 broken at 6900 meters (23,000 feet) at 1200 GMT. Visibility of 4.5 kilometers in haze improved to 9 kilometers by 1000 GMT and decreased to 8 kilometers at 1200 GMT.

Bremen, 79.3 kilometers east of the track center, reported 3/8 decreasing to 1/8 high thin cirrus with visibility 8 to 15 kilometers.

The radiosonde station at Bergen was 149 kilometers east and downstream from the track. The raob showed a warming trend below 400 millibars and cooler above than the sounding taken six hours earlier.

Synoptic Remarks. The surface chart for 0000 GMT showed an occluded front that extended from north of the Arctic Circle southeast and south to near Oslo then as a cold front southsouthwest through the North Sea to Belgium and off the west coast of Morocco with a wave near Madrid. The front was approaching the flight track and there was southwesterly flow over the track. At 1200 GMT the cold front had passed over the track and was on a line from southern Norway, Bremen, Offenbach, Avignon to Fes. There was a weak cell of high pressure centered two degrees west of Brest. Flow over the track was west-southwesterly. At 500 millibars at 0000 GMT there was weak ridging from northern Italy to northern Scandinavia and a closed low just southeast of Iceland. At 1200 GMT there was ridging from Spain northeastward to Latvia. The track had weak northwesterly flow at this level. The air mass was modified maritime polar. The satellite maps for 1259 and 1309 GMT showed thin clouds over all of western Europe and a frontal system approaching Great Britain.

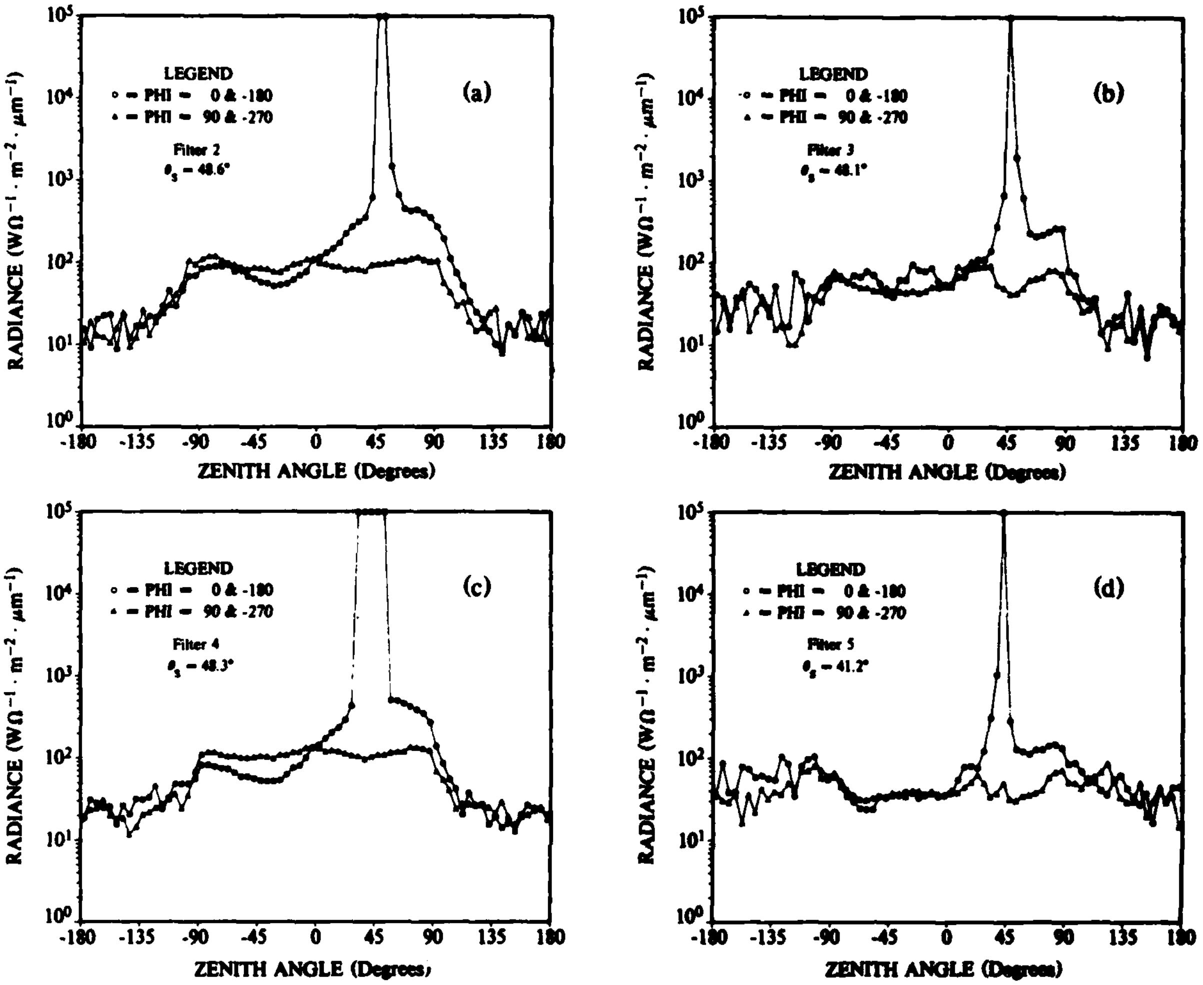

Fig. 5-4. Sky and terrain radiances - Meppen, Germany. Flight C-468, altitude ~ 270m AGL.

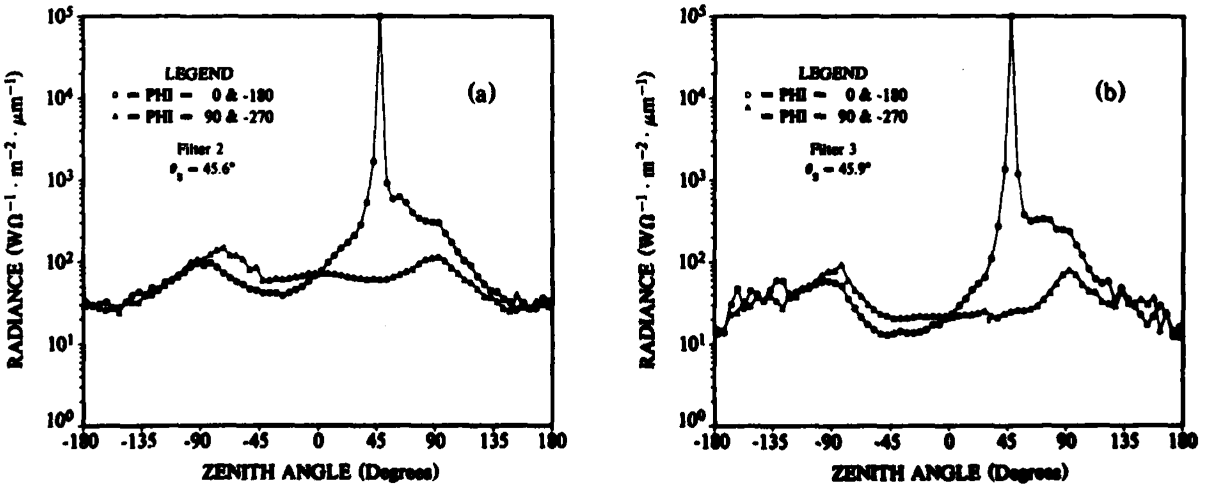

Fig. 5-5. Sky and terrain Radiances - Meppen, Germany. Flight C-468, altitude ~ 1400m AGL.

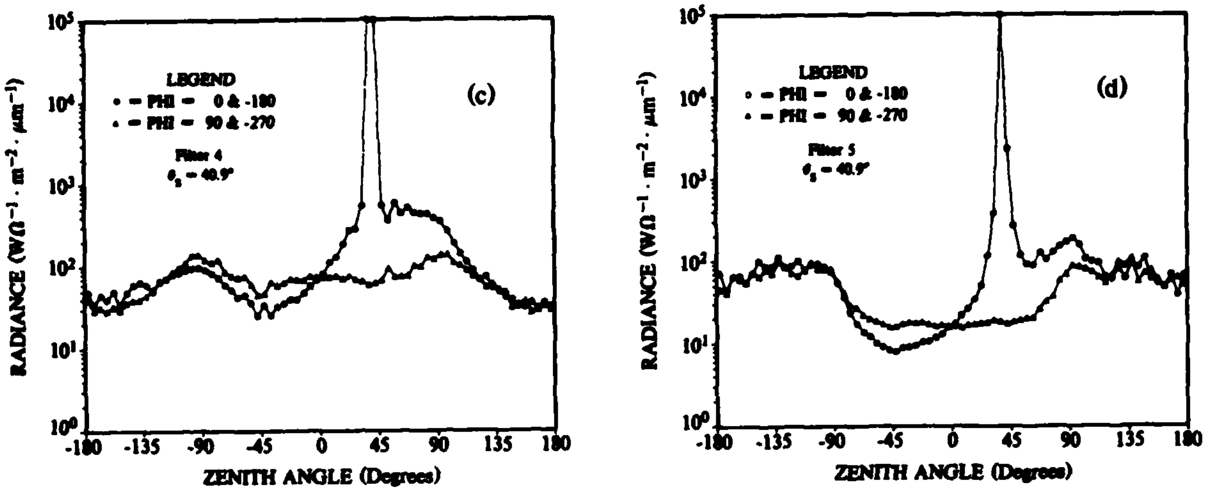

Fig. 5-5 (con't). Sky and terrain Radiances - Meppen, Germany. Flight C-468, altitude ~ 1400m AGL.

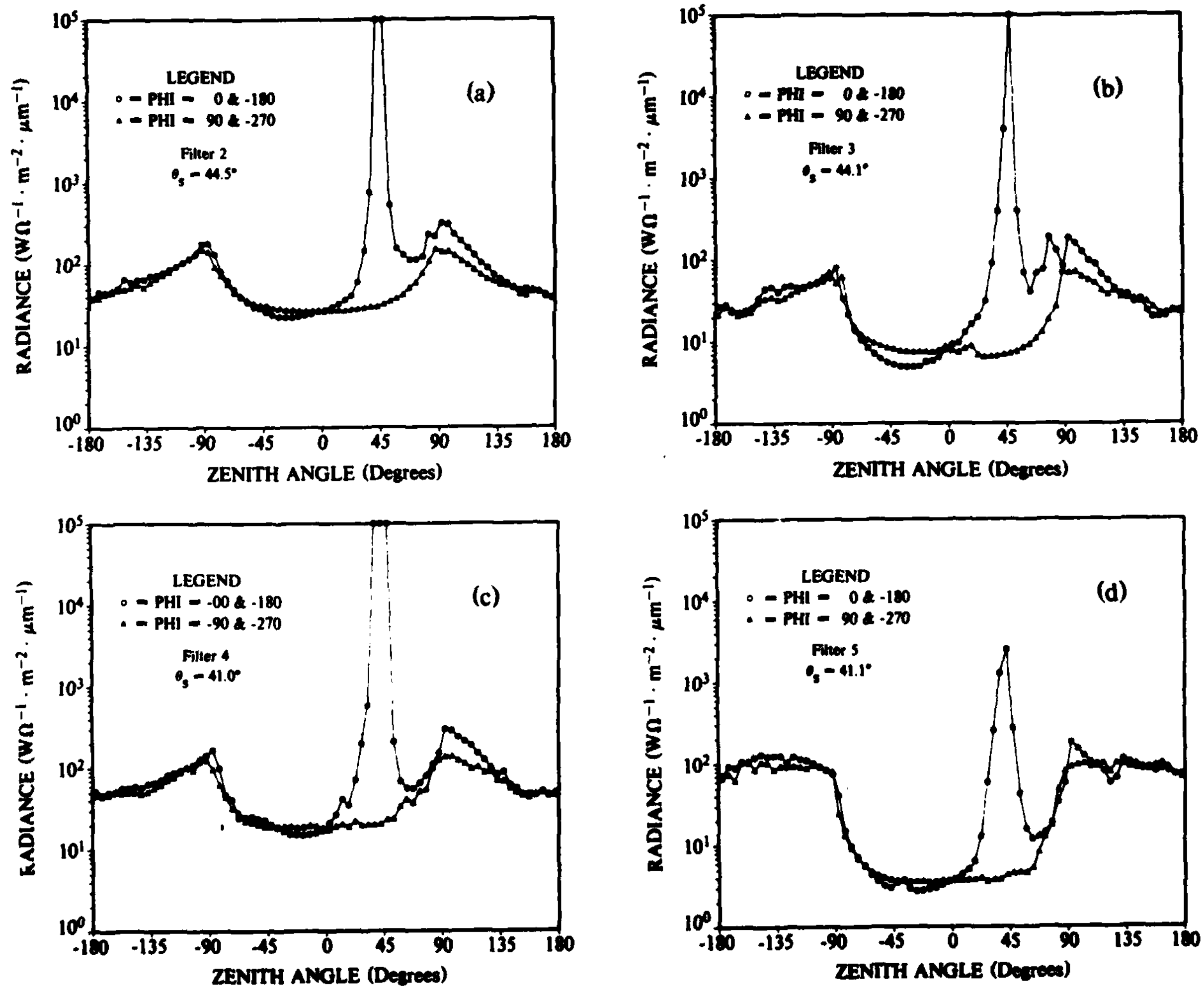

Fig. 5-6. Sky and terrain Radiances - Meppen, Germany. Flight C-468, altitude ~ 3100m AGL.

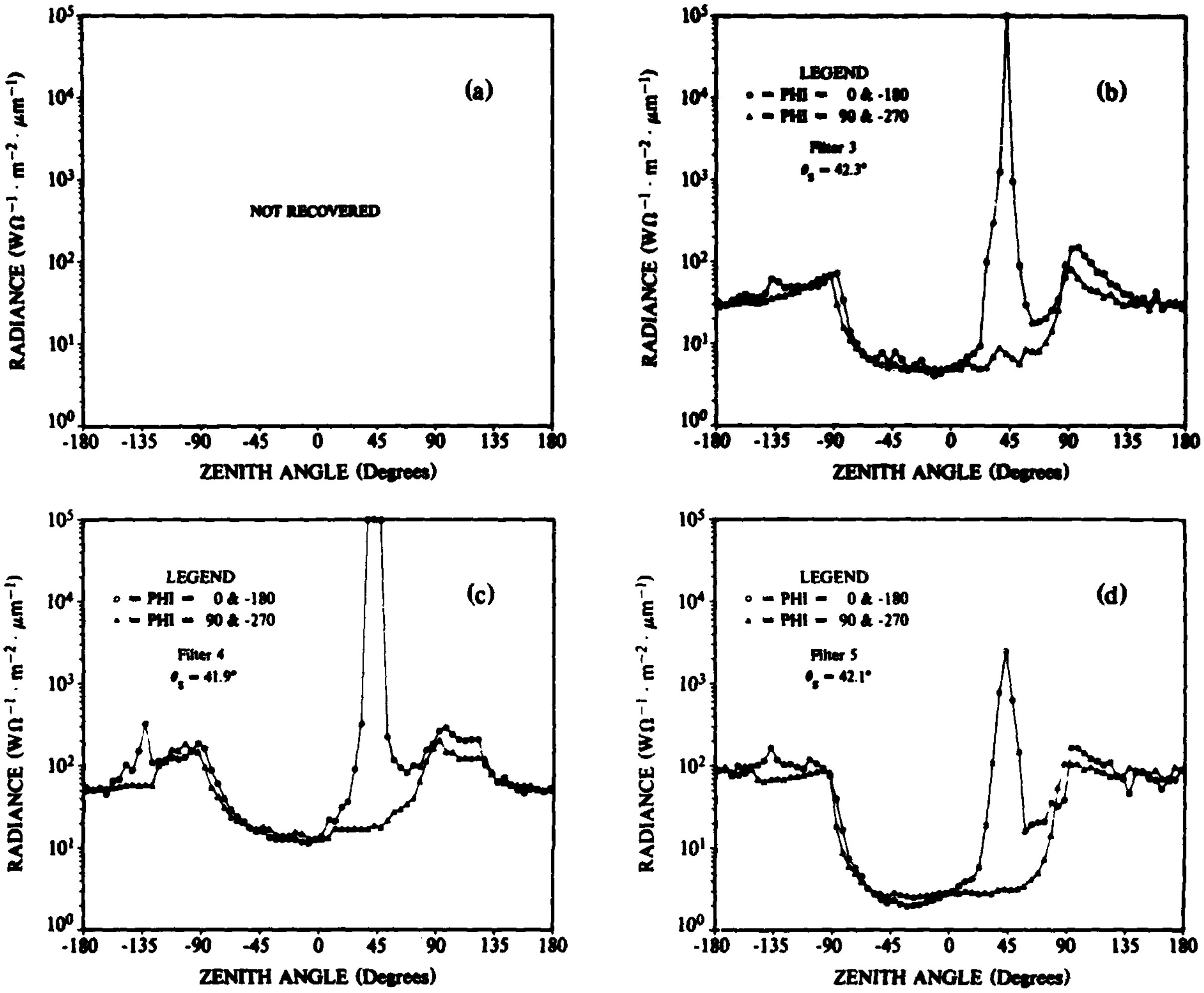

Fig. 5-7. Sky and terrain Radiances - Meppen, Germany. Flight C-468, altitude ~ 6000m AGL.

6. SUMMARY

A data set which contains nearly 500 arrays representing measurements of sky and terrain radiance values is described and illustrated. The measurements were made using radiometer systems mounted on a C-130 aircraft during a series of European flights associated with the NATO program OPAQUE, Fenn (1978) and Johnson *et al.* (1979).

Radiance measurements throughout the 4π field surrounding the aircraft were made in four spectral bands having mean wavelengths of 478, 557, 664 and 765nm. Spectral sets of measurements were made at each of several altitudes between the surface and approximately 6 km AGL.

Evaluation of the data illustrates good orientation and radiometric accuracies, except for stray light influences as the radiometer field of view swept near and through the solar disc. Corrective procedures are outlined and their application is undergoing further refinement.

These data are appropriate for use in the development of operationally useful predictive models as illustrated in Hering (1981). The radiance data in conjunction with their companion scattering coefficient data, Johnson and Gordon (1980) are readily applicable to the determination of slant path contrast transmittances, atmospheric optical depths, aerosol directional scattering characteristics, flux divergences and their attendant determinations of turbid atmospheric single scattering albedos.

7. ACKNOWLEDGEMENTS

This report has been prepared for the Air Force Geophysics Laboratory under Contract No. F19628-78-C-0200. The author wishes to thank the members of the Visibility Laboratory technical staff for their assistance in

preparing these data, and in particular to acknowledge the contributions of Mr. Nils R. Persson, our senior computer specialist, and Ms. Alicia G. Hill and Mr. John C. Brown our specialists in computer assisted document preparation. The corrective techniques and their supporting analyses represent major contributions by Ms. Jacqueline I. Gordon and Mr. Wayne S. Hering

8. REFERENCES

Barteneva, O. D. (1960), "Scattering Functions of Light in the Atmospheric Boundary Layer," Bull. Acad. Sci. U.S.S.R., Geophysics Series, 1237-1244.

Deirmendjian, D. (1969), "Electromagnetic Scattering on Spherical Polydispersions", Elsevier, New York.

Duntley, S. Q., R. W. Johnson, J. I. Gordon, and A. R. Boileau (1970), "Airborne Measurements of Optical Atmospheric Properties at Night", University of California at San Diego, Scripps Institution of Oceanography, Visibility Laboratory, SIO Ref. 70-7, AFCRL-70-0137.

Duntley, S. Q., R. W. Johnson, J. I. Gordon (1972), "Airborne and Ground Based Measurements of Optical Atmospheric Properties in Central New Mexico", University of California at San Diego, Scripps Institution of Oceanography, Visibility Laboratory, SIO Ref. 72-71, AFCRL-72-0461.

Duntley, S. Q., R. W. Johnson, and J. I. Gordon (1975), "Airborne Measurements of Optical Atmospheric Properties, Summary and Review II", University of California at San Diego, Scripps Institution of Oceanography, Visibility Laboratory, SIO Ref. 75-26, AFCRL-TR-75-0457.

Duntley, S. Q., R. W. Johnson, and J. I. Gordon (1976), "Airborne Measurements of Optical Atmospheric Properties in Northern Germany", University of California at San Diego, Scripps Institution of Oceanography, Visibility Laboratory, SIO Ref. 76-17, AFGL-TR-76-0188.

Duntley, S. Q., R. W. Johnson, J. I. Gordon (1977), "Airborne Measurements of Atmospheric Volume Scattering Coefficients in Northern Europe, Spring 1976", University of California, San Diego, Scripps Institution of Oceanography, Visibility Laboratory, SIO Ref. 77-8, AFGL-TR-77-0078.

Duntley, S. Q., R. W. Johnson, and J. I. Gordon (1978a), "Airborne Measurements of Atmospheric Volume Scattering Coefficients in Northern Europe, Fall 1976", University of California at San Diego, Scripps Institution of Oceanography, Visibility Laboratory, SIO Ref. 78-3, AFGL-TR-77-0239.

Duntley, S. Q., R. W. Johnson, and J. I. Gordon (1978b), "Airborne Measurements of Atmospheric Volume Scattering Coefficients in Northern Europe, Summer 1977", University of California at San Diego, Scripps Institution of Oceanography, Visibility Laboratory, SIO Ref. 78-28, AFGL-TR-78-0168.

Duntley, S. Q., R. W. Johnson, and J. I. Gordon (1978c), "Airborne Measurements of Optical Atmospheric Properties, Summary and Review III", University of California at San Diego, Scripps Institution of Oceanography, Visibility Laboratory, SIO Ref. 79-5, AFGL-TR-78-0286.

Fenn, R. W. (1978), "OPAQUE - A Measurement Program on Optical Atmospheric Quantities in Europe, Vol. I The NATO OPAQUE Program", Special Reports No. 211, AFGL-TR-78-0011.

Hering, W. S. (1981), "An Operational Technique for Estimating Visible Spectrum Contrast Transmittance", University of California at San Diego, Scripps Institution of Oceanography, Visibility Laboratory, SIO Ref. 82-1 AFGL-TR-81-0198.

Irvine, W. M. (1968), "Multiple Scattering by Large Particles II Optically Thick Layers", Astrophys. J., 152, 823-834.

Johnson, F. S. (1954), "The Solar Constant", Journal of Meteorology 11, 431-439.

Johnson, R. W., W. S. Hering, J. I. Gordon, B. W. Fitch, and J. S. Shields (1979), "Preliminary Analysis & Modelling Based Upon Project OPAQUE Profile and Surface Data", University of California at San Diego, Scripps Institution of Oceanography, Visibility Laboratory, SIO Ref. 80-5, AFGL-TR-79-0285.

Johnson, R. W. and J. I. Gordon (1979), "Airborne Measurements of Atmospheric Volume Scattering Coefficients in Northern Europe, Winter 1978", University of California, San Diego, Scripps Institution of Oceanography, Visibility Laboratory, SIO Ref. 79-25, AFGL-TR-79-0159.

Johnson, R. W. and J. I. Gordon (1980), "Airborne Measurements of Atmospheric Volume Scattering Coefficients in Northern Europe, Summer 1978", University of California at San Diego, Scripps Institution of Oceanography, Visibility Laboratory, SIO Ref. 80-20, AFGL-TR-80-0207.

Johnson, R. W. (1981), "Winter and Summer Measurements of European Very Low Altitude Volume Scattering Coefficients," University of California, San Diego, Scripps Institution of Oceanography, SIO Ref. 81-00, AFGL-TR-81-0154.

Johnson, R. W. and W. S. Hering (1981), "Measurements of Optical Atmospheric Quantities in Europe and Their Application to Modelling Visible Spectrum Contrast Transmittance", Paper presented at the 29th Symposium of the AGARD Electromagnetic Wave Propagation Panel on Special Topics in Optical Propagation, Monterey, California (April, 1981). AGARD-CP-300.

Kattawar, G. W. (1975), "A Three-Parameter Analytic Phase Function for Multiple Scattering Calculations", J. Quant. Spectrosc. Radiat. Transfer, Vol. 15, pp. 839-849, Pergamon Press, Oxford.

APPENDIX A: Meteorological Glossary & Abbreviations

SKY AND CEILING

Sky cover symbols are in ascending order. Figures preceding symbols are heights in hundreds of feet above station. Sky cover symbols are:

○	Clear: less than 0.1 sky cover
⦶	Scattered: 0.1 to less than 0.6 sky cover
⦷	Broken: 0.6 to 0.9 sky cover
⊕	Overcast: more than 0.9 sky cover
-	Thin (when prefixed); light (when suffixed)
--	Very light (when suffixed)
-X	Partial obscuration: 0.1 to less than 1.0 sky hidden by precipitation or obstruction to vision (bases at surface)
X	Obscuration: 1.0 sky hidden by precipitation or obstruction to vision (bases at surface)

Letter preceding height of layer identifies ceiling layer and indicates how ceiling height was obtained. Thus:

A	Aircraft
B	Balloon (pilot or ceiling)
D	Estimated height of cirriform clouds on basis of persistency
E	Estimated height of noncirriform clouds
M	Measured
R	Radiosonde balloon or radar
U	Height of cirriform ceiling layer unknown
V	Immediately following numerical value indicates a varying ceiling (also used with varying visibility)
W	Indefinite, sky obscured by surface base phenomenon. e.g. fog, blowing dust, snow

RELATIVE HUMIDITY (RH)

Reported in percent and computed from temperature and dewpoint.

VISIBILITY (VV)

Reported in kilometers.

WEATHER AND OBSTRUCTION TO VISION SYMBOLS

A	Hail	IF	Ice fog
AP	Small hail	K	Smoke
BD	Blowing dust	L	Drizzle
BN	Blowing sand	R	Rain
BS	Blowing snow	RW	Rain showers
D	Dust	S	Snow
E	Sleet	SG	Snow grains
EW	Sleet showers	SP	Snow pellets
F	Fog	SW	Snow showers
GF	Ground fog	T	Thunderstorms
H	Haze	ZL	Freezing drizzle
IC	Ice crystals	ZR	Freezing rain

CLOUD ABBREVIATIONS

Ac	Altocumulus	Cs	Cirrostratus
As	Altostratus	Cu	Cumulus
Cb	Cumulonimbus	Ns	Nimbostratus
Cc	Cirrocumulus	Sc	Stratocumulus
Ci	Cirrus	St	Stratus

WIND

Direction in ten's of degrees from true north, speed in meters per second (mps). A "0000" indicates calm. A "G" indicates gusty. A "Q" indicates squall. Peak speed of gusts, when reported, follows G or Q. The contraction WSHFT in remarks followed by time group (GMT) indicates wind shift and its time of occurrence.

Examples: 0109 is 010 degrees, 9 mps.
3607G11 is 360 degrees, 7 mps, peak speed in gusts of 11 mps.

MSG: Data missing in original source.

APPENDIX B (Ref. AFGL-TR-81-0198)

SUMMARY OF INPUT DATA, COMPUTATION STEPS AND RESULTANT DATA

B.1 General Input Data

B.1.1 Number of atmospheric layers

B.1.2 Representative wavelength (μm)

B.1.3 Extraterrestrial solar (lunar) irradiance ($w/m^2\mu m$)

B.1.4 Rayleigh optical depth for top layer for $\lambda = .55\mu m$ (unless otherwise specified, set equal to .0258 for layer base altitude of 10 km).

B.1.5 Solar zenith angles (deg.)

B.1.6 Zenith viewing angles (deg.)

B.1.7 Scattering angles between viewing path and sun (deg., max. 10)

B.1.8 Average reflectance of underlying surface and reflectance of background in the vicinity of target if different than the average reflectance.

B.2 Input Data Each Layer

B.2.1 Base altitude (km)

B.2.2 Scattering mixing ratio

B.2.3 Single scattering albedo

B.3 Computation Steps

B.3.1 Compute Rayleigh atmosphere optical thickness for each layer

B.3.2 Compute total optical thickness for each layer.

B.3.3 Compute optical depth for the base of each layer.

B.3.4 Compute single scattering phase function and asymmetry factors for each layer. (These parameters may be specified if desired in lieu of the use of model algorithms).

B.3.5 Transform optical depth, single scattering albedo, and asymmetry factor in accordance with delta-Eddington approximation.

B.3.6 Compute path function distribution for the base of each sub-layer (each layer is divided equally into 2 sub-layers).

B.3.7 Compute path radiance distribution for each sub-layer.

B.3.8 Compute path transmittance distribution for each sub-layer.

B.3.9 Compute sky/terrain radiance distribution at sub-layer boundaries.

B.3.10 Compute slant path contrast transmittance of selected paths.

B.4 Output Tables and Data

B.4.1 Single scattering phase function, $P(z,\beta)$, as calculated or specified for each layer.

B.4.2 Path radiance, $L^*(z,\theta,\beta)$, for each sub-layer and each solar zenith angle, θ_s.

B.4.3 Path transmittance $T_r(z,\theta)$ for each sub-layer.

B.4.4 Sky radiance, $L_r(z,\theta,\beta)$, for $0° \leqslant \theta \leqslant 85°$ for selected levels (max 5) for each θ_s.

B.4.5 Sky radiance, $L_r(z,\theta,\beta)$ for $95° \leqslant \theta \leqslant 180°$ for selected levels (max 5) for each θ_s.

B.4.6 Sky plus terrain radiance $L_r(z,\theta,\beta)$ for $95° \leqslant \theta \leqslant 180°$ for selected levels (max 5) for each θ_s.

B.4.7 Contrast transmittance, $T_c(z,\theta,\beta)$ between object and sensor altitudes (max. 5 altitude intervals) for $0° \leqslant \theta \leqslant 85°$ and for each θ_s.

B.4.8 Contrast transmittance $T_c(z,\theta,\beta)$ between object and sensor altitudes (max. 5) for $95° \leqslant \theta \leqslant 180°$ and for each θ_s.

B.5 Additional Output From The Supplemental Eddington Computer Program

The standard Eddington computer program is employed as an integrated part of the model calculations of contrast transmittance. The following output from the program as modified by the delta-Eddington transformation of input parameters is available in tabular form for the base of each sub-layer and for each solar zenith angle:

- optical depths, τ and τ'
- components of Eddington diffuse radiance, $L_D(z)$ and $L_{D'}(z)$
- total scalar irradiance
- downward diffuse irradiance
- upward diffuse irradiance
- solar irradiance
- total downward irradiance

APPENDIX C

VISIBILITY LABORATORY CONTRACTS AND RELATED PUBLICATIONS

Previous Related Contracts:
F19628-73-C-0013, F19628-76-C-0004

PUBLICATIONS:

Duntley, S. Q., R. W. Johnson, J. I. Gordon, and A. R. Boileau (1970), "Airborne Measurements of Optical Atmospheric Properties at Night", University of California at San Diego, Scripps Institution of Oceanography, Visibility Laboratory, SIO Ref. 70-7, AFCRL-70-0137.

Duntley, S. Q., R. W. Johnson, and J. I. Gordon (1972a), "Airborne Measurements of Optical Atmospheric Properties in Southern Germany", University of California at San Diego, Scripps Institution of Oceanography, Visibility Laboratory, SIO Ref. 72-64, AFCRL-72-0255.

Duntley, S. Q., R. W. Johnson, and J. I. Gordon (1972b), "Airborne and Ground-Based Measurements of Optical Atmospheric Properties in Central New Mexico", University of California at San Diego, Scripps Institution of Oceanography, Visibility Laboratory, SIO Ref. 72-71, AFCRL-72-0461.

Duntley, S. Q., R. W. Johnson, and J. I. Gordon (1972c), "Airborne Measurements of Optical Atmospheric Properties, Summary and Review", University of California at San Diego, Scripps Institution of Oceanography, Visibility Laboratory, SIO Ref. 72-82, AFCRL-72-0593.

Duntley, S. Q., R. W. Johnson, and J. I. Gordon (1973), "Airborne Measurements of Optical Atmospheric Properties in Southern Illinois", University of California at San Diego, Scripps Institution of Oceanography, Visibility Laboratory, SIO Ref. 73-24, AFCRL-TR-73-0422.

Duntley, S. Q., R. W. Johnson, and J. I. Gordon (1974), "Airborne and Ground-Based Measurements of Optical Atmospheric Properties in Southern Illinois", University of California at San Diego, Scripps Institution of Oceanography, Visibility Laboratory, SIO Ref. 74-25, AFCRL-TR-74-0298.

Duntley, S. Q., R. W. Johnson, and J. I. Gordon (1975a), "Airborne Measurements of Optical Atmospheric Properties in Western Washington", University of California at San Diego, Scripps Institution of Oceanography, Visibility Laboratory, SIO Ref. 75-24, AFCRL-TR-75-0414.

Duntley, S. Q., R. W. Johnson, and J. I. Gordon (1975b), "Airborne Measurements of Optical Atmospheric Properties, Summary and Review II", University of California at San Diego, Scripps Institution of Oceanography, Visibility Laboratory, SIO Ref. 75-26, AFCRL-TR-75-0457.

Duntley, S. Q., R. W. Johnson, and J. I. Gordon (1976), "Airborne Measurements of Optical Atmospheric Properties in Northern Germany", University of California at San Diego, Scripps Institution of Oceanography, Visibility Laboratory, SIO Ref. 76-17, AFGL-TR-76-0188.

Duntley, S. Q., R. W. Johnson, and J. I. Gordon (1977), "Airborne Measurements of Atmospheric Volume Scattering Coefficients in Northern Europe, Spring 1976", University of California at San Diego, Scripps Institution of Oceanography, Visibility Laboratory, SIO Ref. 77-8, AFGL-TR-77-0078.

Duntley, S. Q., R. W. Johnson, and J. I. Gordon (1978a), "Airborne Measurements of Atmospheric Volume Scattering Coefficients in Northern Europe, Fall 1976", University of California at San Diego, Scripps Institution of Oceanography, Visibility Laboratory, SIO Ref. 78-3, AFGL-TR-77-0239.

Duntley, S. Q., R. W. Johnson, and J. I. Gordon (1978b), "Airborne Measurements of Atmospheric Volume Scattering Coefficients in Northern Europe, Summer 1977", University of California at San Diego, Scripps Institution of Oceanography, Visibility Laboratory, SIO Ref. 78-28, AFGL-TR-78-0168.

Duntley, S. Q., R. W. Johnson, and J. I. Gordon (1978c), "Airborne Measurements of Optical Atmospheric Properties, Summary and Review III", University of California at San Diego, Scripps Institution of Oceanography, Visibility Laboratory, SIO Ref. 79-5, AFGL-TR-78-0286.

Fitch, B. W. (1981), "Measurements of Aerosol Size Distribution in the Lower Troposphere over Northern Europe", University of California at San Diego, Scripps Institution of Oceanography, Visibility Laboratory, SIO Ref. 81-18, AFGL-TR-80-0192.

Gordon, J. I., J. L. Harris, Sr., and S. Q. Duntley (1973), "Measuring Earth-to-Space Contrast Transmittance from Ground Stations", Appl. Opt. 12, 1317-1324.

Gordon, J. I., C. F. Edgerton, and S. Q. Duntley (1975), "Signal-Light Nomogram", J. Opt. Soc. Am. 65, 111-118.

Gordon, J. I., (1979), "Daytime Visibility, A Conceptual Review", University of California at San Diego, Scripps Institution of Oceanography, Visibility Laboratory, SIO Ref. 80-1, AFGL-TR-79-0257.

Hering, W. S. (1981), "An Operational Technique for Estimating Visible Spectrum Contrast Transmittance", University of California at San Diego, Scripps Institution of Oceanography, Visibility Laboratory, SIO Ref. 82-1 AFGL-TR-81-0198.

Johnson, R. W., and J. I. Gordon (1979). "Airborne Measurements of Atmospheric Volume Scattering Coefficients in Northern Europe, Winter 1978", University of California at San Diego, Scripps Institution of Oceanography, Visibility Laboratory, SIO Ref. 79-25, AFGL-TR-79-0159.

Johnson, R. W., W. S. Hering, J. I. Gordon, B. W. Fitch, and J. S. Shields (1979), "Preliminary Analysis & Modelling Based Upon Project OPAQUE Profile and Surface Data", University of California at San Diego, Scripps Institution of Oceanography, Visibility Laboratory, SIO Ref. 80-5, AFGL-TR-79-0285.

Johnson, R. W. and J. I. Gordon (1980), "Airborne Measurements of Atmospheric Volume Scattering Coefficients in Northern Europe, Summer 1978", University of California at San Diego, Scripps Institution of Oceanography, Visibility Laboratory, SIO *Ref. 80-20, AFGL-TR-80-0207.*

Johnson, R. W. (1981a), "Winter and Summer Measurements of European Very Low Altitude Volume Scattering Coefficients," University of California, San Diego, Scripps Institution of Oceanography, SIO Ref. 81-00, AFGL-TR-81-0154.

Johnson, R. W. (1981b), "Spring and Fall Measurements of European Very Low Altitude Volume Scattering Coefficients", University of California at San Diego, Scripps Institution of Oceanography, Visibility Laboratory, SIO Ref. 81-00, AFGL-TR-81-0237.

Johnson, R. W. (1981c), "Daytime Visibility and Nephelometer Measurements Related to its Determination", *ATMOSPHERIC ENVIRONMENT*, 15, 10/11, 1835.

Shields, J. E. (1981), "An Analysis of Infrared and Visible Atmospheric Extinction Measurements in Europe", University of California, San Diego, Scripps Institution of Oceanography, Visibility Laboratory, SIO Ref. 00-00, AFGL-TR-81-0251.